EFFECTS OF TEMEPRATURE GRADIENTS ON TRANSVERSE OSCILLATIONS OF SOLAR MAGNETIC FLUX TUBES

by

SHILPA SUBRAMANIAM

Presented to the Faculty of the Graduate School of

The University of Texas at Arlington in Partial Fulfillment

of the Requirements

for the Degree of

MASTER OF SCIENCE IN PHYSICS

THE UNIVERSITY OF TEXAS AT ARLINGTON

December 2006

ACKNOWLEDGEMENTS

I would like to thank my research advisor, Dr. Zdzislaw Musielak, for his guidance and ideas which lead to this interesting thesis. My appreciations to him for being extremely patient and supportive in helping me learn the subject. I am indebted to him for giving me hints to write my report and for reviewing it. I would like to express gratitude to Dr. John Fry, for agreeing to be in my thesis committee. I would like to express thanks to Dr. James Horwitz for taking the time to review my report and being in my thesis committee. I would also like to thank Dr. Manfred Cuntz for taking time to read my report and giving me his comments. I would also like to thank the staff of the Department of Physics at UTA for all their help.

My appreciation to Vikram Pujari for his moral support and constant encouragement. Finally I would like to thank my parents for having faith in my abilities and encouraging me to follow my dreams. None of this would be possible without them.

This work was supported by NSF Grant ATM-0538278.

November 27, 2006

ABSTRACT

EFFECTS OF TEMPERATURE GRADIENTS ON TRANSVERSE OSCILLATIONS OF SOLAR MAGNETIC FLUX TUBES

Publication No. _____

Shilpa Subramaniam, M.S.

The University of Texas at Arlington, 2006

Supervising Professor: Dr. Zdzislaw Musielak

Solar magnetic flux tubes support three fundamental modes: longitudinal, transverse and torsional tube waves. Previous studies showed that the propagation of longitudinal and transverse waves along thin and isothermal magnetic flux tubes is affected by the cutoff frequency, which are global quantities that restricts the wave propagation to only those frequencies that are higher than the cutoff. It was also demonstrated that the tubes respond to freely propagating longitudinal and transverse tube waves by oscillating at the corresponding cutoff frequency. No cutoff frequency

was found for torsional waves propagating along thin and isothermal magnetic flux tubes. Since the solar atmosphere is not isothermal, the effects of different temperature gradients on the cutoff for transverse tube waves are investigated. It is shown that this cutoff frequency becomes a local quantity and its physical meaning is different than the global cutoff. The obtained results are used to explain the observed frequencies of oscillations of solar magnetic flux tubes.

TABLE OF CONTENTS

LIST OF ILLUSTRATIONS

CHAPTER 1

INTRODUCTION

1.1 The Sun

The Sun is the most important star in the sky for us because its output of light and heat supports life on Earth [3]. The upper atmosphere of the Earth is heavily influenced by the Sun's ultraviolet and X-ray emission [3]. Solar-terrestrial research is important because it studies the influence of the Sun's variable output on the Earth's magnetosphere and upper atmosphere. Probing and understanding the Sun will help us in analyzing other stellar systems as well [49].

Our Sun is an average main-sequence star. The Sun maintains its size by balancing two competing forces: gravity pulling inward and gas and radiation pressure pulling outward; this force balance is called hydrostatic equilibrium [3]. The Sun contains about 99.85% of the solar system's mass and it is a huge ball of plasma held together by gravity [3].

1.1.1 Structure of the Sun

There is a lot of interest in the solar interior particularly because we can now probe it by helioseismology and neutrino observations. Since detailed observations can be done for the Sun, they are essential for the general understanding of all stars [10].

Different layers of the Sun are identified as the core, radiation zone, convection zone, photosphere, chromosphere and the corona. The core is the most inner layer

which has a temperature of 15 million Kelvin. The density is the highest there and is about 100 times of the density of water [3]. The pressure is 200 billion times that on the surface of the Earth. Energy is generated by the process of nuclear fusion in which hydrogen is converted into helium. The energy produced in the core today will take about a million years to reach the surface [3].

The radiation zone is the layer above the core where energy is primarily transported by means of radiation. The radiation zone stretches to about 70% of the Sun's radius. The temperature decreases to 10 million Kelvin and the density also decreases. The layer above this is the convection zone where the temperature reduces to 2 million Kelvin while the density also decreases. Energy is transported by means of convection which is a more efficient process to transport energy than radiation. Convection occurs because hot gas is less dense than cool gas. The rising of hot plasma and sinking of cool plasma form a cycle that transports energy from the convection zone to the solar surface [3].

The photosphere is above the convection zone and it is the lowest of the three layers comprising the Sun's atmosphere. Its temperature is approximately 6000 Kelvin and it decreases outward [3]. The density also decreases. Most of the light that we see from the Sun is comes from this layer. Most of the energy produced in the core finally leaves as thermal radiation from the photosphere [3]. This layer is marked throughout by the bubbling pattern of granulation produced by the underlying convection. There granules typically measure about 1000 km across [49].

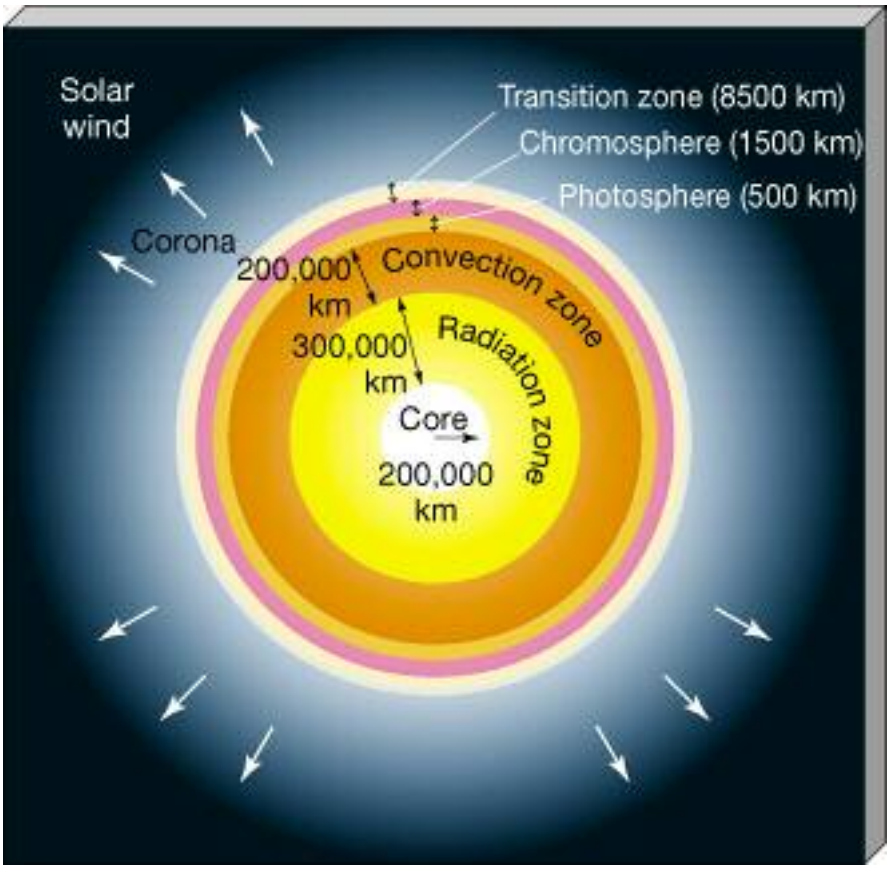

Figure 1.1 Structure of the Sun [3].

The chromosphere is the layer above the photosphere. The chromospheric temperature rises to about 10000 Kelvin while density continues to drop. This is the primary source of ultraviolet radiation. Studies have revealed that the chromosphere has numerous spikes which are jets of hot gases called spicules, and they are located at the boundaries of supergranules. A typical supergranule has approximately a diameter the size of the Earth [3].

There is a region between the solar corona and the chromosphere called transition region where the temperature goes up significantly while the density continues to drop. The solar corona is the uppermost layer of the Sun's atmosphere in

which the temperature is around 1 million Kelvin. However, the density is very low. This layer is the source of X-rays. The corona expands outward to become solar wind at great distances from the Sun [3].

1.1.2 The Chromosphere

The chromosphere is a region between the temperature minimum and the corona. The magnetic field dominates the gas motions in this region. Compared to the chaos of the granulation, the chromosphere shows an ordered structure governed by the magnetic pattern of the photosphere. Velocities and oscillations here are greater in magnitude than in the photosphere but are controlled by the field. It has been observed that the heating of the chromosphere-corona takes place over magnetically enhanced regions. Higher in the atmosphere, the contrast between regions of strong magnetic field and the rest of the Sun becomes very important [3], [10], [49].

1.1.3 The Heating Problem

The high temperatures of the chromosphere and corona have been a puzzle to scientists. It is generally believed that the Sun's strong magnetic fields carry energy upward from the solar surface to the chromosphere and corona. The rising and falling gases in the convection zone shakes magnetic field lines beneath the solar surface causing waves to be generated along the magnetic field lines that carry energy upward to the solar atmosphere. The precise mechanism by which this is done is still not completely understood [47].

1.1.4 Role of Magnetic Field

The Sun would have been a very dull star had it not been for the existence of magnetic fields. The Sun's magnetic field is not distributed uniformly but concentrated in flux ropes which appear on the surface as sunspots, plages and network.

It is believed that the effects of differential rotation and convection motion are responsible for generating strong magnetic fields in the Sun. Magnetic fields trap and guide the plasma. The solar plasma can move freely along magnetic field lines but cannot easily move perpendicular to them. The solar magnetic field is responsible for many features observed on the Sun like sunspots, plages, filaments, prominences and coronal mass ejections [10], [49].

1.2 Magnetohydrodynamics (MHD)

MHD is the study of electrically conducting fluids and their interactions with magnetic fields. The electrically conducting fluid is usually an ionized gas called plasma.

1.2.1 Plasma

Plasma is the fourth state of matter. When the temperature is increased, atoms lose their electrons. This is called ionization. The splitting of the gas into electrons and ions makes it electrically conducting. Although it is composed of electrons, ions and other neutral particles, it is electrically neutral. These particles have very high energy. Plasma conducts electrical current and generates magnetic fields. It is the most common form of matter. This state of matter is found in the Sun and other stars. Examples of this state on Earth are the ionosphere, auroras, lasers and gas discharges [20].

1.2.2 Fluid description of a Plasma

Liquids and gases can be characterized by quantities like density, pressure, velocity and temperature. The fluid is treated as a continuous and macroscopic medium i.e., the behavior of a large number of molecules is considered. Since the Plasma is an electrically conducting medium, there are a few more quantities used to characterize its electrical properties like charge density, current density, electric field and magnetic field.

1.2.3 MHD model

The ideal MHD model provides a single fluid description of low-velocity, long-wavelength, or low-frequency, macroscopic plasma behavior. It is assumed that only weak electric fields are present because electrons and ions can easily recombine. The fundamental equations used in MHD are Maxwell's Equations, Ohm's Law and equations of Fluid Dynamics [15].

These above assumptions transform the full Maxwell's equations to low frequency Maxwell's equations. This is accomplished by neglecting the displacement current and the net charge. We can neglect displacement current because the MHD waves under consideration have velocities much slower than the speed of light [20].

1.2.4 MHD Equations

The ideal MHD model is governed by the following set of equations

$$\frac{\partial \rho}{\partial \mathrm{t}} + \nabla . \rho \vec{v} = 0 \tag{1.1}$$

$$\rho \frac{dv}{dt} = \vec{J} \times \vec{B} - \nabla p + \rho \vec{g} \tag{1.2}$$

$$\frac{d}{dt}\left(\frac{p}{\rho^{\gamma}}\right)=0 \tag{1.3}$$

These equations describe the conservation of mass (Equation 1.1), momentum (Equation 1.2) and energy (Equation 1.3) respectively; where p is the pressure. The continuity equation implies that the total number of plasma particles is conserved. The momentum equation describes a fluid with three interacting forces : the pressure gradient force ∇p, the magnetic force $\vec{J}\times\vec{B}$,and the inertial force $\rho\frac{dv}{dt}$ are present. The energy equation represents an adiabatic evolution given by a ratio of specific heats γ=5/3. Another relation is the generalized Ohm's Law, given by

$$\vec{J}=\lambda_{el}\left(\vec{E}+\vec{v}\times\vec{B}\right) \tag{1.4}$$

Ohm's Law implies that plasma is a perfect conductor. It is this assumption that gives the ideal characteristics to the MHD equations [20]. For ideal plasma, the conductivity is infinite and so we can rewrite the generalized Ohm's Law as

$$\vec{E}+\vec{v}\times\vec{B}=0 \tag{1.5}$$

where λ_{el} is the conductivity of the unmagnetized plasma.

The other equations are the low frequency Maxwell equations discussed earlier.

$$\nabla\times\vec{E}=-\frac{\partial\vec{B}}{\partial t} \tag{1.6}$$

$$\nabla\times\vec{B}=\mu_0\vec{J} \tag{1.7}$$

$$\nabla\cdot B=0 \tag{1.8}$$

We obtain the conservation law of the magnetic field by using generalized Ohm's law and the induction equation as

$$\frac{\partial \vec{B}}{\partial t} - \nabla \times \left(\vec{v} \times \vec{B} \right) = \frac{c^2}{4\pi\lambda_{el}} \nabla^2 \vec{B} \tag{1.9}$$

For a plasma at rest, we can get an equation that is a special condition of equation (1.9) and we can write this diffusion equation as

$$\frac{\partial \vec{B}}{\partial t} = \frac{c^2}{4\pi\lambda_{el}} \nabla^2 \vec{B} \tag{1.10}$$

We can also develop the equation that describes the forces exerted on the plasma by the magnetic field. For this we first consider the Lorentz force $\vec{F}$, acting on a charge q in $\vec{E}$ and $\vec{B}$ fields, given by

$$\vec{F} = q\vec{E} + \frac{q}{c} \vec{v} \times \vec{B} \tag{1.11}$$

The force density is given by $\vec{f}$ = $\vec{F}$/V, where V is the volume, and so for the MHD approximation we can write this density as

$$\vec{F} = \frac{1}{c} \vec{J} \times \vec{B} = -\frac{1}{4\pi} \vec{B} \times \left(\nabla \times \vec{B} \right) = -\nabla \frac{\overrightarrow{B}^2}{8\pi} + \frac{1}{4\pi} \left(\vec{B} . \nabla \right) \vec{B} \tag{1.12}$$

The final magnetohydrodynamic equations are obtained by using the equations derived earlier [see Equations. (1.1) to (1.4)]. These equations are

$$\frac{\partial \rho}{\partial t} + \nabla \cdot \rho \vec{v} = 0 \tag{1.13}$$

$$\rho \left(\frac{\partial \vec{v}}{\partial t} + \vec{v} \cdot \nabla \vec{v} \right) = -\nabla p - \frac{1}{4\pi} \vec{B} \times \left(\nabla \times \vec{B} \right) - \rho \vec{g} \tag{1.14}$$

$$\frac{\partial \vec{B}}{\partial t} - \nabla \times \left(\vec{v} \times \vec{B} \right) = 0 \tag{1.15}$$

$$\frac{\partial S}{\partial t} + \vec{v} \cdot \nabla S = \left. \frac{dS}{dt} \right|_R \tag{1.16}$$

$$\frac{\partial}{\partial t}\left(\frac{1}{2}\rho v^2 + \rho \vec{E} + p\varphi + \frac{B^2}{8\pi} \right) = -\nabla \left\{ \rho \vec{v} \left(\frac{1}{2} v^2 + \vec{E} + \frac{p}{\rho} + \varphi \right) + \vec{P} \right\} + \rho T \left. \frac{dS}{dt} \right|_{ext'} \tag{1.17}$$

The last equation represents the conservation of energy. The total energy is the sum of kinetic, internal, potential and magnetic energy density. S stands for entropy and $\vec{P}$ is the Poynting vector. The last term on the right hand side of equation (1.17) gives the change in entropy caused by energy flowing into the volume element from the external medium. A system satisfying the MHD equations is known as magnetofluid [14], [15].

1.2.5 MHD Waves

The presence of a magnetic field in the plasma defines a direction within the plasma. Thus the wave propagation speed and its properties depend on the direction in which the wave is propagating relative to the magnetic field. Because of the high electric conductivity of solar plasma, magnetic field lines follow plasma flows called a frozen-in effect. The speed of propagation and the frozen-in effect by the magnetic field gives rise to three different waves, which can be classified as fast, intermediate and slow depending on the magnitudes of their speeds of propagation [19].

The intermediate waves are also called Alfvén waves. This wave is a purely transverse wave. There is no change in the magnitude of the magnetic field but only in the direction of the field because the change in magnetic field is perpendicular to the original field. The only other changes are in the tangential velocity and the direction of

the magnetic field. The phase velocity is equal to the Alfvén velocity (see Equation 1.19). This wave is a purely magnetohydrodynamic wave which depends on the magnetic field and the density of the plasma [19].

The MHD equations derived in section 1.2.4 have to be supplemented by an equation of state relating the pressure to the density. These equations can be linearized in small quantities by neglecting the second and higher order terms, and can be solved by taking the Fourier transform in time and space. The result is the following dispersion relation [19]

$$\left(\omega^2 - k^2 {c_A}^2\right)\left[\omega^4 - \omega^2 k^2 \left({c_S}^2 + {c_A}^2\right) + k^4 {c_S}^2 {c_A}^2\right] = 0 \tag{1.18}$$

where

$${c_A}^2 = \frac{{B_0}^2}{4\pi\rho_0} \tag{1.19}$$

k is the wave number, ω is the wave frequency and $B_0^{\,2}/4\pi\rho_0$ is the magnetic pressure. This velocity is called Alfvén velocity. Typically Alfvén velocity is much lower than the speed of sound. However it can become very large if the density is very small or if the magnetic field is very strong. We also know that the speed of sound is given by

$${c_s}^2 = \gamma \frac{p_0}{\rho_0} \tag{1.20}$$

For the background magnetic field to be uniform, there exist three distinct propagation modes for small amplitude waves. The characteristic phase velocities can be derived for each of the magnetoacoustic modes and they are given by

$$c_A^{\,2} = \frac{B_0^{\,2}}{4\pi\rho_0} = \frac{B_0^{\,2}\cos^2\theta}{4\pi\rho_0} \tag{1.21}$$

$$c_F^{\,2} = \frac{1}{2}\left(c_S^{\,2} + c_A^{\,2}\right) + \frac{1}{2}\left[\left(c_S^{\,2} + c_A^{\,2}\right)^2 - 4c_S^{\,2}c_A^{\,2}\cos^2\theta\right]^{1/2} \tag{1.22}$$

$$c_{SL}^{\,2} = \frac{1}{2}\left(c_S^{\,2} + c_A^{\,2}\right) - \frac{1}{2}\left[\left(c_S^{\,2} + c_A^{\,2}\right)^2 - 4c_S^{\,2}c_A^{\,2}\cos^2\theta\right]^{1/2} \tag{1.23}$$

where $c_F^{\,2}$ and $c_{SL}^{\,2}$ are the fast and slow mode phase velocities respectively.

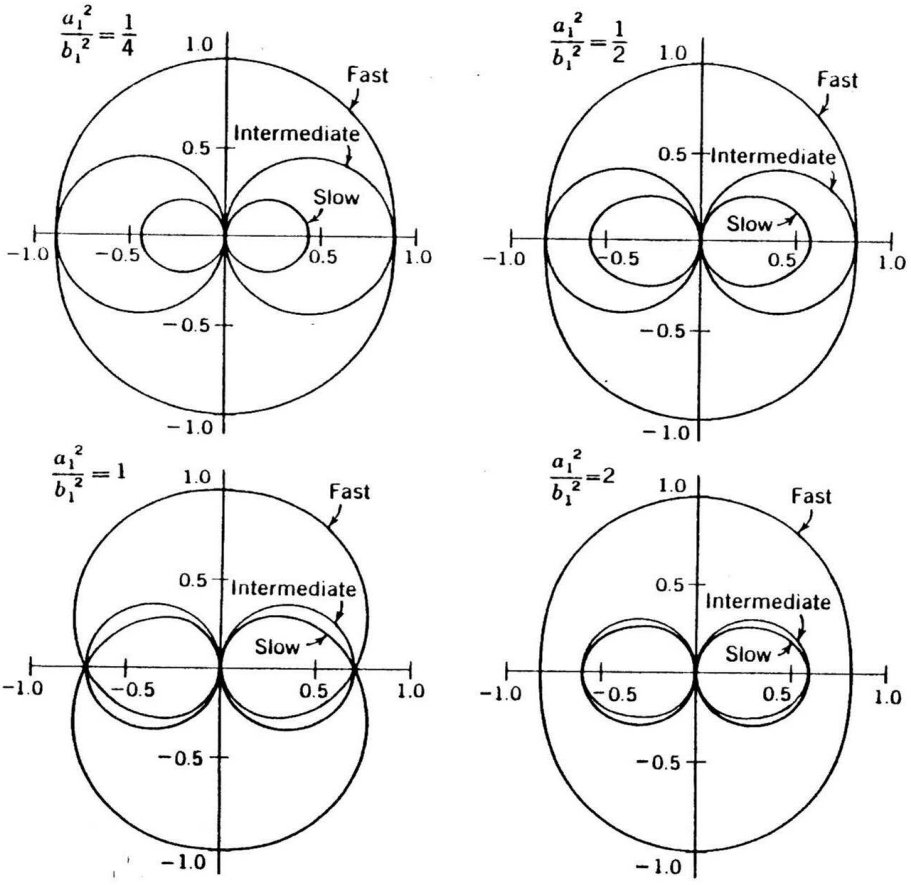

Figure 1.2 Friedrichs diagram for MHD Waves [19].

The fast wave always travels with a speed that is greater than or equal to the intermediate speed or the Alfvén velocity. The slow wave travels with a speed lower than or equal to the intermediate speed. The characteristic speeds of MHD waves can be plotted for several ratios of c_S to c_A as shown in Fig. 1.2. The plots are given in the form suggested by Friedrichs K.O (1954) and is a polar plot showing the dependence of the propagation speeds of the three linear-wave modes on the angle between the wave normal and the magnetic field, for several values of ratio of the sound speed c_S (in this plot denoted by 'a') to the Alfvén velocity c_A (in this plot denoted by 'b').

When the propagation is along the magnetic field, the slow speed is either c_S or c_A, depending on which is smaller. Thus, for $c_S < c_A$, the Alfvén and fast speeds are equal for this direction of propagation and for $c_S > c_A$, the Alfvén and slow speeds are equal. For propagation across the magnetic field, changes in velocity across the three waves are in mutually perpendicular directions. In the limit, $c_S \to c_A$, the fast propagation speed reduces to that of ordinary sound wave and thus approach a pure longitudinal wave. In the same limit, the slow wave becomes a purely transverse wave and approaches the Alfvén speed. When $c_S \to c_A$, the waves do not break up into purely longitudinal and transverse waves. The slow wave becomes purely transverse for propagation across the magnetic field and purely longitudinal for propagation along the magnetic field. On the other hand, fast wave behaves as purely longitudinal for propagation across the magnetic field and as purely transverse for propagation along the magnetic field [19].

CHAPTER 2

MAGNETIC FLUX TUBES

2.1 Introduction

There is a close relationship between solar activity and the presence of magnetic fields, and are many processes are responsible for this. However, they occur on such a small scale that they are difficult to observe. Recently new techniques have aided us to resolve the magnetic flux tubes, which represent the largest magnetic field concentration in the solar photosphere outside sunspots [10], [49].

It is now accepted that the solar photosphere has many regions of vertical magnetic fields which we call a magnetic flux tube. Their field strength is typically in the kilogauss range and has diameters of the order of 100km. These occur in the magnetic network which is located at the boundary of supergranules.

Magnetic flux tubes may be thought of as communication channels that connect one part of the Sun to another. These tubes are very efficient in transferring the non-radiative energy to the solar atmosphere from the convective layers existing beneath the solar surface [10], [49].

2.1.1 Granulation

Granulation is observed in the photosphere. This layer is easier to study than the unseen layers below and transparent layers above. The photosphere has a fairly uniform surface roughened by granulation and is the layer that we observe as the surface of the

Sun. It is connected with the convection zone below by the granulation which are irregular polygons in shape. They have a lifetime of a few minutes and are affected only by strong magnetic fields.

If the magnetic field strength exceeds gas pressure, the material is constrained to move along field lines and should exhibit the regular structure characteristic of magnetic fields. A flow pattern called supergranulation is caused by a large scale convective pattern. In these cells, the material flows outward from the center, sweeping magnetic fields to the cell boundaries, where magnetic flux tubes and down flow are observed [10].

2.1.2 Convective Collapse

When the magnetic flux tube emerges at the solar surface, a down-flow is initiated by radiation cooling. This flow is then accelerated by the instability caused by this flow which decreases the pressure inside the tube as shown in Fig. 2.1. But this increases the field strength and makes the tube stable. Therefore, the instability is self-limiting and after a finite displacement the flow stops and leaves the tube in a state of equilibrium. This suggests that a magnetic flux tube is held together by a balance between the outward pressure of the field and the inward force caused by a lower gas pressure inside the flux tube [10], [49].

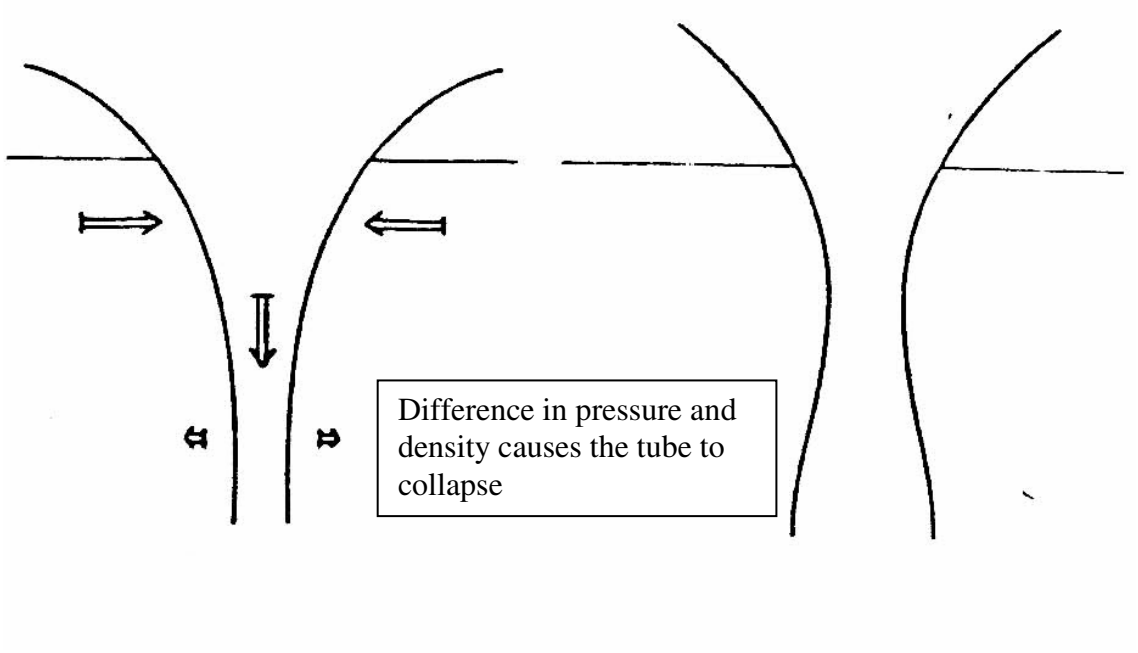

Figure 2.1 Convective Collapse [42].

2.1.3 Magnetohydrodynamics of thin flux tubes

The magnetic field at the solar surface is observed to be highly inhomogeneous. It consists of certain areas where the fields are strong and certain areas where they are essentially field free. We refer to this region of strong magnetic field as a flux tube if it is observed outside sunspots. At the photospheric level, some of these flux tubes can be treated as thin flux tubes, hence, the thin flux tube approximation is a very useful treatment for theoretical studies [10].

2.1.3.1 Assumptions for a thin flux tube

A simplified model can be constructed by assuming the tube to be very slender. It is assumed that their diameter changes very slowly along their length. They are almost vertically oriented. The field intensity B is taken to be uniform across the flux

tube. The electrical conductivity is assumed to be infinite because of the frozen-in field condition and the perturbations are considered to be adiabatic. As the tube is thin, it is always in pressure equilibrium with the surroundings [10], [20], [49].

The horizontal pressure balance is given by

$$P_0 + \left(\frac{B_0^{\,2}}{8\pi} \right) = P_e \tag{2.1}$$

where P_0 and B_0 are the unperturbed gas pressure and field strength at some point inside the tube and P_e is the external gas pressure. This shows that the tube can be in equilibrium only if the internal gas pressure is less than the external gas pressure. We can define a parameter β as

$$\beta = 8\pi P / B^2 \tag{2.2}$$

If β is taken as magnetic intensity within a flux tube and P is the gas pressure, then $\beta \approx 1$ near the photosphere and $\beta < 1$ above the photosphere because the gas pressure decreases exponentially. When $\beta < 1$, the field expands to fill the space so that the field lines confined to the flux tubes at the photosphere begin to diverge with height and fill the entire volume of the solar chromosphere [39].

2.1.4 Modes of a thin flux tube

The wave modes of a thin flux tube are simple to visualize. There are three different modes in a thin tube as shown in Fig. 2.2 . An untwisted tube of circular cross section has two modes called transversal (kink mode) and longitudinal (sausage) mode. If a twist is included then a third mode called torsional mode exists [39].

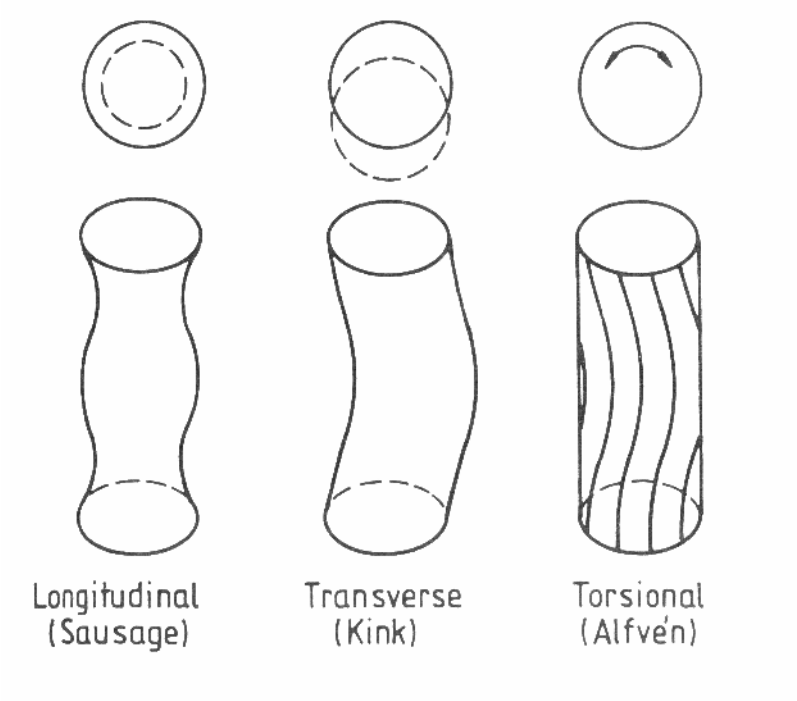

Figure 2.2 The modes in a thin flux tube.

The torsional mode propagates at Alfvén velocity. For this mode, there is no interaction between the mode and the surroundings of the tube as the boundary of the tube is not perturbed. This mode is not affected by motions outside the tube and it does not distort the shape of the tube. This is however not the case for both longitudinal and transverse modes [39].

The polarization of the longitudinal mode wave is parallel while that for both the transverse and torsional modes is perpendicular. The longitudinal wave travels with a speed less than both the sound speed and the Alfvén velocity of the tube. The transverse wave travels with a speed that is lower than the Alfvén velocity inside the

tube. The torsional wave propagates with the Alfvén velocity inside the tube, which means that it has the fastest speed among the three modes [39].

CHAPTER 3

MODES OF OSCILLATIONS IN A MAGNETIC FLUX TUBE

Analysis of the Sun's interior and atmosphere by the study of restoring forces suggests the presence of four main wave modes, namely sound waves, gravity waves, Alfvén waves and plasma oscillations [10]. Sound waves have been observed directly in the photosphere and indirect evidence suggests their presence in the chromosphere as well [10]. The restoring force for Alfvén waves is the tension in magnetic field lines and evidence has been found for their presence in the corona and solar wind. Solar gravity waves are predicted to be present in the Sun's radiative core and their restoring force is the buoyancy of the fluid. Due to difficulties in observing them at the photosphere, it is believed that these waves should be heavily damped in the intervening convective layers in accordance with theoretical studies [49]. Information on plasma oscillations is obtained by observing radio waves and the restoring force for them is the electrostatic attraction between ions and electrons in plasma [10].

3.1 Basic Formulation and Assumptions

Solar convection zones are the main source of non-radiative energy required to heat solar chromospheres and coronae; where the wave energy is generated by turbulent convection [32]. In non-magnetic regions of convection zones, the non-radiative energy is carried mainly by acoustic waves. In magnetic regions, which are usually identified with solar magnetic flux tubes, three types of waves can be generated: longitudinal,

transverse and torsional [42]; all these have been studied comprehensively in the literature [35].

It is assumed that an isolated magnetic flux tube is embedded in a region with no magnetic field and an isothermal medium. The tube is thin, untwisted, and oriented vertically with circular cross-section, and in temperature equilibrium with the surroundings [31]. A Cartesian coordinate system is chosen with z-axis along the tube axis. Then gravity is

$$\vec{g} = -g\hat{z} \tag{3.1}$$

The magnetic field inside the tube is given by

$$\vec{B}_0 = B_0(z)\hat{z} \tag{3.2}$$

The magnetic field outside the tube is

$$\vec{B}_e = 0 \tag{3.3}$$

The horizontal pressure balance is given by

$$p_0 + (B_0^2 / 8\pi) = p_e \tag{3.4}$$

where p_0 and p_e are the internal and external gas pressures. Magnetic flux conservation and horizontal pressure balance lead to exponentially spreading tube geometry. Because the tube is vertically oriented, the generation of the three different waves can be separated [31]. It has been recognized that it is easier to generate transverse waves than longitudinal waves [40] and that the transverse waves carry more energy than the longitudinal waves [32].

3.2 Excitation by longitudinal tube waves

The outer solar atmosphere oscillates with a period that is different from that of the solar photosphere, specifically the chromosphere is dominated by 3 min oscillations and are observed in the interior of the supergranulation cells [5], [7], [36]. The response of exponentially diverging magnetic flux tubes in an isothermal solar atmosphere to the propagation of longitudinal tube waves produced in the solar convection has been studied analytically [26]. The authors approached the problem by casting the derived equation into a Klein-Gordon form, which explicitly gives the cutoff frequency and is solved by using Laplace transforms.

3.2.1 Klein Gordon equation and cutoff frequency

The tube is modeled by introducing velocity perturbation, magnetic field perturbation, density perturbation and pressure perturbation as [26]

$$\vec{v} = v_z(z,t)\hat{z} \tag{3.5}$$

$$\vec{b} = b_z(z,t)\hat{z} \tag{3.6}$$

$$\rho = \rho(z,t) \tag{3.7}$$

$$p = p(z,t) \tag{3.8}$$

Then we linearize the basic MHD equations, apply the thin flux approximation and derive the wave equation for the velocity perturbation [32] as,

$$\frac{\partial^2 v_z}{\partial t^2} - c_L^2 \frac{\partial^2 v_z}{\partial t^2} + \frac{c_L^2}{2H}\frac{\partial v_z}{\partial z} + \frac{c_L^2}{H^2}\left(\frac{1}{2} - \frac{1}{2\gamma} + \frac{c_s^2}{c_A^2}\frac{\gamma - 1}{\gamma^2}\right)v_z = 0 \tag{3.9}$$

where the tube velocity is given by

$$c_L = \frac{c_s c_A}{\sqrt{c_s^2 + c_A^2}} \tag{3.10}$$

and c_s is the speed of sound , c_A is the Alfvén velocity, and H is the pressure scale height. The tube velocity is a constant in this model because both c_s and c_A are constant and the form of the derived equation is the same for each wave variable [26].

Next we cast the above velocity perturbation equation in the form Klein-Gordon equation by introducing $v_z(z,t) = v(z,t)\sqrt{B_0/\rho_0}$ which gives

$$\left[\frac{\partial^2}{\partial t^2} - c_L^2 \frac{\partial^2}{\partial z^2} + \Omega_L^2\right] v(z,t) = 0 \tag{3.11}$$

where Ω_L is the cutoff frequency for longitudinal tube waves [8] given by

$$\Omega_L = \frac{c_L}{H}\left(\frac{9}{16} - \frac{1}{2\gamma} + \frac{c_s^2}{c_A^2}\frac{\gamma - 1}{\gamma^2}\right)^{1/2} \tag{3.12}$$

3.3 Excitation by transverse tube waves

We can analyze transverse tube waves using the same method as that for longitudinal tube waves, with the assumptions given in section 3.1 [30] . It is assumed that the transverse tube waves are excited by external turbulence alone and that there are no other motions inside or outside the tube, so the generated perturbations of the tube velocity is given by $\vec{v}(z,t) = v_x(z,t)\hat{x}$ and the magnetic field by $\vec{b}(z,t) = b_x(z,t)\hat{x}$ [30]. The total magnetic field in the Cartesian coordinate system is given by [30] , $\vec{B}_0 = B_0(z)\hat{z} + b_x(t,x)\hat{x}$ with $b_x / B_0 = l_x$

3.3.1 Klein Gordon equation and cutoff frequency

The momentum equation for velocity v is [31],

$$\rho_0 \frac{\partial \vec{v}}{\partial t} = -\nabla\left(p_0 + \frac{B_0^2}{8\pi} \right) + \frac{1}{4\pi}\left(\vec{B}_0.\nabla\right)\vec{B}_0 + \rho_0 \vec{g} \tag{3.13}$$

where p_0 is the gas pressure, ρ_0 the density and $\vec{B}_0$ the magnetic field and all the above quantities are inside the tube.

Next we obtain the momentum equation outside the tube for the turbulent motions with a velocity u,

$$\rho \frac{\partial \vec{u}}{\partial t} = -\nabla p + \rho \vec{g} \tag{3.14}$$

where ρ is the total external gas density and p is the total external gas pressure.

Then the horizontal pressure balance is used to relate the momentum equation inside and outside the tube. We then derive the wave equation for velocity perturbation by linearizing the MHD equations using $\nabla.\vec{v} = 0$ and $\left(\vec{v}.\nabla\right)\vec{v} = 0$ and then apply the thin flux tube approximation [31] to obtain,

$$\frac{\partial^2 v_x}{\partial t^2} - c_T^2 \frac{\partial^2 v_x}{\partial z^2} + \frac{c_T^2}{2H}\frac{\partial v_x}{\partial z} = 0 \tag{3.15}$$

where the characteristic velocity of these transverse waves is given by

$$c_T = \frac{B_0}{\sqrt{4\pi(\rho_0 + \rho_e)}} \tag{3.16}$$

The first derivative is removed from the above equation by using $v_x = v/\rho_0^{1/4}$ to obtain

$$\left[\frac{\partial^2}{\partial t^2} - c_T^2 \frac{\partial^2}{\partial z^2} + \Omega_T^2\right] v(z,t) = 0 \tag{3.17}$$

where Ω_T is the cutoff frequency for transverse tube waves [42] given by,

$$\Omega_T = \frac{c_T}{4H} \tag{3.18}$$

where H is the pressure (density) scale height. This characteristic speed can also be written in terms of the sound speed as

$$c_T = \frac{c_s}{\sqrt{\gamma(\beta + 1/2)}} \tag{3.19}$$

3.4 Excitation by torsional tube waves

Propagation of torsional waves has been studied extensively in literature using different approaches [37]. However no conclusive results for the existence of cutoff frequency for torsional have been obtained [29]. The dispersion relation was derived to be [29],

$$\omega^2 = \left(k_z^2 + 2k_z k_\varsigma + k_\varsigma\right) c_A^2 \tag{3.20}$$

Where ω is the wave frequency and k_z and k_ς are the z and ς components of the wave vector $\vec{k}$, respectively. Now, defining $\kappa = k_z + k_\varsigma$ and write

$$\omega^2 = \kappa^2 c_A^2 \tag{3.21}$$

which shows that the propagation of linear torsional waves along thin and isothermal magnetic tube waves is not affected by any cutoff frequency [29]. It has been shown that this non-existence of a cutoff frequency for torsional tube waves is independent of the choice of the coordinate system and the wave variables.

CHAPTER 4

EFFECTS OF TEMPERATURE GRADIENTS ON TRANSVERSE TUBE WAVES

So far the study of oscillations in a magnetic flux tube assumed a background medium that was isothermal and stratified for simplicity of analysis and was called an isothermal atmosphere [21]. However this simplification has its limitations and so for getting a complete picture we need to consider a non-isothermal atmosphere. A method to determine the cutoff frequencies for linear transverse tube waves' propagating in a non-isothermal medium is developed based on wave variable transformation [28]. The derived wave equations are then cast as Klein-Gordon equations to determine the critical frequency [24]; after which turning point frequencies are determined by applying the oscillation theorem. Then, we can determine the cutoff frequency by using physical arguments to pick the largest frequency. This generalized method can be applied to any model and in our case we have modeled the non-isothermal atmosphere by power law temperature gradient models.

4.1 Basic Formulation and Assumptions

It is assumed that an isolated magnetic flux tube is embedded in a region with no magnetic field and a non-isothermal medium. The tube is thin, untwisted, and oriented vertically with circular cross-section, and in temperature equilibrium with the surroundings. A Cartesian coordinate system is chosen with z-axis along the tube axis.

We linearize the MHD equations and obtain the equations of motion for the tube. The linear transverse tube waves are described by the perturbed quantities $\rho = 0$, $p = 0$, $\vec{v}(z,t) = v_x(z,t)\hat{x}$ and $\vec{b}(z,t) = b_x(z,t)\hat{x}$. The momentum equation of the oscillating tube is

$$\rho_0 \frac{\partial \vec{v}}{\partial t} + \nabla\left(p_0 + \frac{B_0^2}{8\pi} \right) - \rho_0 \vec{g} - \frac{1}{4\pi}\left(\vec{B}_0.\nabla\right)\vec{B}_0 - \frac{1}{4\pi}\left(\vec{B}_0.\nabla\right)\vec{b}_0 = 0 \tag{4.1}$$

The equation of motion of the fluid outside the tube with a velocity u is

$$\rho_e \frac{\partial \vec{u}}{\partial t} + \nabla p_e - \rho_e \vec{g} = 0 \tag{4.2}$$

Then the above two can be combined to write the momentum equation as

$$\frac{\partial v_x}{\partial t} - \frac{B_0}{4\pi(\rho_0 + \rho_e)} \frac{\partial b_x}{\partial z} = 0 \tag{4.3}$$

The x-component of the induction equation is

$$\frac{\partial b_x}{\partial t} - B_0 \frac{\partial v_x}{\partial z} = 0 \tag{4.4}$$

4.1.1 Wave Equations

We then combine Equation (4.3) and (4.4) to obtain

$$\frac{\partial^2 v_x}{\partial t^2} - \frac{B_0^2}{4\pi(\rho_0 + \rho_e)} \frac{\partial^2 v_x}{\partial z^2} - \frac{B_0^2}{4\pi(\rho_0 + \rho_e)} \frac{B_0'}{B_0} \frac{\partial v_x}{\partial z} = 0 \tag{4.5}$$

where $B_0' = dB_0 / dz$. (4.6)

Defining $c_T^2 \equiv \frac{B_0^2}{4\pi(\rho_0 + \rho_e)}$ (4.7)

We then define the pressure scale height by using the following

$$c_{se}^2(z) \equiv c_s^2(z) \tag{4.8}$$

$$\frac{1}{H_e(z)} \equiv \frac{1}{H(z)} = \frac{\gamma g}{c_s^2(z)} \tag{4.9}$$

The pressure scale height is then given by

$$\frac{B_0'(z)}{B_0(z)} = -\frac{1}{2H(z)} \tag{4.10}$$

The wave equation for velocity is then given by

$$\frac{\partial^2 v_x}{\partial t^2} - c_T^2(z)\frac{\partial^2 v_x}{\partial z^2} + \frac{c_T^2(z)}{2H(z)}\frac{\partial v_x}{\partial z} = 0 \tag{4.11}$$

Next we obtain the wave equation for magnetic field in a similar way as

$$\frac{\partial^2 b_x}{\partial t^2} - c_T^2(z)\frac{\partial^2 b_x}{\partial z^2} - \left(2\frac{(dc_T/dz)}{c_T(z)} + \frac{1}{2H(z)}\right)\frac{\partial b_x}{\partial z} = 0 \tag{4.12}$$

4.1.2 Klein - Gordon Equations

We then transform the derived wave equations into τ-space by using the transformation [24],

$$d\tau = \frac{dz}{c_T} \tag{4.13}$$

Introducing $v = v(t,\tau)$ and $b = b(t,\tau)$ lets us modify Equations (4.12) and (4.13) as

$$\frac{\partial^2 v}{\partial t^2} - \frac{\partial^2 v}{\partial \tau^2} + \left[\frac{c_T}{2H} + \frac{c_T'}{c_T}\right]\frac{\partial v}{\partial \tau} = 0 \tag{4.14}$$

$$\frac{\partial^2 b}{\partial t^2} - \frac{\partial^2 b}{\partial \tau^2} - \left[\frac{c_T}{2H} + \frac{c_T'}{c_T}\right]\frac{\partial b}{\partial \tau} = 0 \tag{4.15}$$

where $c_T^{'} \equiv \frac{dc_T}{d\tau}$ (4.16)

To remove the first-order derivatives from (4.15) and (4.16), we use

$v(t,\tau) = \tilde{v}(t,\tau)e^{\zeta/2}$ (4.17)

and $b(t,\tau) = \tilde{b}(t,\tau)e^{\zeta/2}$ (4.18)

where $\zeta = \int_0^{\tau}\left[\frac{c_T(\tilde{\tau})}{2H(\tilde{\tau})} + \frac{c_T^{'}(\tilde{\tau})}{c_T(\tilde{\tau})}\right]d\tilde{\tau}$ (4.19)

This is simplified further and then we obtain

$$\Omega_v^2(\tau) = \frac{c_T^2}{16H^2} + \frac{3}{4}\left(\frac{c_T^{'}}{c_T}\right)^2 + \frac{1}{4}\frac{c_T H^{'}}{H^2} - \frac{1}{2}\frac{c_T^{''}}{c_T} \quad (4.20)$$

$$\Omega_b^2(\tau) = \frac{c_T^2}{16H^2} - \frac{1}{4}\left(\frac{c_T^{'}}{c_T}\right)^2 - \frac{1}{4}\frac{c_T H^{'}}{H^2} + \frac{1}{2}\frac{c_T^{''}}{c_T} + \frac{1}{2}\frac{c_T^{'}}{H} \quad (4.21)$$

The Klein-Gordon equation for velocity is then given by

$$\frac{\partial^2\tilde{v}}{\partial t^2} - \frac{\partial^2\tilde{v}}{\partial\tau^2} + \Omega_v^2(\tau)\tilde{v} = 0 \quad (4.22)$$

The Klein-Gordon equation for magnetic field is

$$\frac{\partial^2\tilde{b}}{\partial t^2} - \frac{\partial^2\tilde{b}}{\partial\tau^2} + \Omega_b^2(\tau)\tilde{b} = 0 \quad (4.23)$$

In an isothermal medium, $c_T^{'} = 0$, $c_T^{''} = 0$ and $H^{'} = 0$ which gives us

$\Omega_v = \Omega_b = \frac{c_T}{4H}$ (Spruit's cutoff frequency) (4.24)

4.2 Cutoff Frequencies for Power Law Non-isothermal Models

We now consider a temperature gradient with a power law model and derive the corresponding critical frequencies for both velocity and magnetic field. Then we use the oscillation theorem and perform Fourier Transform in time to obtain the corresponding turning point frequencies [28]. The cutoff frequency is determined from them by choosing the one that is the larger of the two because in order to have a propagating transverse tube wave, the wave frequency must always be higher than the turning point frequency. Thus the waves propagating at a height z, will be propagating only if their frequency is higher than the cutoff frequency corresponding to that height.

4.2.1 Cutoff Frequency for Case m = 1

We begin by deriving equations for the case when m = 1 and then we consider the case when m = 2 and the general case of m > 2 in the subsequent sections. We begin by considering the following temperature gradient

$$T_0(\xi) = T_{00}\xi \tag{4.25}$$

This gives the following

$$c_s^2(\xi) = c_{S0}^2\xi \tag{4.26}$$

$$H(\xi) = H_0\xi \tag{4.27}$$

$$c_T^2(\xi) = c_{T0}^2\xi \tag{4.28}$$

$$B_0^2(\xi) = B_{00}^2\xi^{-z_0/H_0} \tag{4.29}$$

$$\tau = 2\frac{z_0}{c_{T0}}\xi^{1/2} \tag{4.30}$$

$$\xi = \frac{1}{4}\frac{c_{T0}^2}{z_0^2}\tau^2 \tag{4.31}$$

Now we calculate $c_T(\tau)$, $H(\tau)$ and their derivatives as

$$c_T(\tau) = \frac{1}{2}\frac{c_{T0}^2}{z_0}\tau \tag{4.32}$$

$$H(\tau) = \frac{1}{4}\frac{c_{T0}^2}{z_0^2}H_0\tau^2 \tag{4.33}$$

$$\frac{c_T^2}{H^2} = 4\left(\frac{z_0}{H_0}\right)^2\frac{1}{\tau^2} \tag{4.34}$$

$$\left(\frac{c_T'}{c_T}\right)^2 = \frac{1}{\tau^2} \tag{4.35}$$

$$\frac{c_T H'}{H^2} = 4\left(\frac{z_0}{H_0}\right)\frac{1}{\tau^2} \tag{4.36}$$

$$\left(\frac{c_T''}{c_T}\right) = 0 \tag{4.37}$$

We now obtain the critical frequencies [27] using Equations (4.20-4.21)

$$\Omega_v^2(\tau) = \left[\frac{1}{4}\left(\frac{z_0}{H_0}\right)^2 + \left(\frac{z_0}{H_0}\right) + \frac{3}{4}\right]\frac{1}{\tau^2} \tag{4.38}$$

$$\Omega_b^2(\tau) = \left[\frac{1}{4}\left(\frac{z_0}{H_0}\right)^2 - 1\right]\frac{1}{\tau^2} \tag{4.39}$$

4.2.1.1 Turning Point Frequencies

The next step is to perform the Fourier Transform of Equations (4.22 -4.23) in time, we get

$$\frac{d^2\tilde{v}}{d\tau^2} + \left(\omega^2 - \Omega_v^2\right)\tilde{v} = 0 \tag{4.40}$$

$$\frac{d^2\tilde{b}}{d\tau^2} + \left(\omega^2 - \Omega_b^2\right)\tilde{b} = 0 \tag{4.41}$$

Now we apply the Oscillation Theorem to obtain the turning point frequencies, which separate propagating and non-propagating wave solutions [16]. According to this theorem, one can compare the form of a given equation to another one whose solutions are known, to obtain the turning point frequencies (see Appendix A). So here, we compare the steady-state Klein-Gordon equations to Euler's equation and then determine frequencies that correspond to turning point of these equations. The turning point frequencies are

$$\Omega_{tp,v}^2(\tau) = \Omega_v^2(\tau) + \frac{1}{4}\frac{1}{\tau^2} \tag{4.42}$$

$$\Omega_{tp,b}^2(\tau) = \Omega_b^2(\tau) + \frac{1}{4}\frac{1}{\tau^2} \tag{4.43}$$

Using this in (4.38 and 4.39) we get

$$\Omega_{tp,v}^2(\tau) = \left[1 + \left(\frac{z_0}{H_0}\right) + \frac{1}{4}\left(\frac{z_0}{H_0}\right)^2\right]\frac{1}{\tau^2} \tag{4.44}$$

$$\Omega_{tp,b}^2(\tau) = \frac{1}{4}\left(\frac{z_0}{H_0}\right)^2\frac{1}{\tau^2} \tag{4.45}$$

Comparing (4.44) and (4.45) we can say that $\Omega_{tp,v}^2 > \Omega_{tp,b}^2$ and so

$\Omega_{cutoff} = \Omega_{tp,v}^{1/2}$, which in terms of ξ (using 4.30) is

$$\Omega_{cutoff}(\xi) = \frac{1}{2}\frac{c_{T0}}{z_0}\left[1+\left(\frac{z_0}{H_0}\right)+\frac{1}{4}\left(\frac{z_0}{H_0}\right)^2\right]^{1/2}\frac{1}{\xi^{1/2}}$$

that can be simplified further using $\Omega_0 \equiv \frac{c_{T0}}{4H_0}$ to

$$\Omega_{cutoff}(\xi) = \Omega_0\left[1+4\left(\frac{H_0}{z_0}\right)+4\left(\frac{H_0}{z_0}\right)^2\right]^{1/2}\frac{1}{\xi^{1/2}} \tag{4.46}$$

4.2.2 Cutoff Frequency for Case m = 2

Now we consider another power law modeled with m = 2 and derive the turning point frequency. We begin by considering the following temperature gradient

$$T_0(\xi) = T_{00}\xi^2 \tag{4.47}$$

This gives the following

$$c_s^2(\xi) = c_{S0}^2\xi^2 \tag{4.48}$$

$$H(\xi) = H_0\xi^2 \tag{4.49}$$

$$c_T^2(\xi) = c_{T0}^2\xi^2 \tag{4.50}$$

$$B_0^2(\xi) = B_{00}^2 e^{z_0/H_0\xi} \tag{4.51}$$

$$\tau = \frac{z_0}{c_{T0}}\ln\xi \tag{4.52}$$

$$\xi = e^{\frac{c_{T0}\tau}{z_0}} \tag{4.53}$$

Now we calculate $c_T(\tau)$, $H(\tau)$ and their derivatives as

$$c_T(\tau) = c_{T0}e^{c_{T0}\tau/z_0} \tag{4.54}$$

$$H(\tau) = H_0 e^{(2c_{T0}\tau)/z_0} \tag{4.55}$$

$$\frac{c_T}{H} = \frac{c_{T0}}{H_0} e^{-c_{T0}\tau/z_0} \tag{4.56}$$

$$\left(\frac{c_T^{'}}{c_T}\right)^2 = \left(\frac{c_{T0}}{z_0}\right)^2 \tag{4.57}$$

$$\frac{c_T H^{'}}{H^2} = 2\frac{c_{T0}^2}{z_0 H_0} e^{-c_{T0}\tau/z_0} \tag{4.58}$$

$$\left(\frac{c_T^{''}}{c_T}\right) = \left(\frac{c_{T0}}{z_0}\right)^2 \tag{4.59}$$

We now obtain the critical frequencies using Equations (4.20-4.21)

$$\Omega_v^2(\tau) = \left(\frac{c_{T0}}{4H_0}\right)^2 \left[4\left(\frac{H_0}{z_0}\right)^2 + 8\left(\frac{H_0}{z_0}\right) e^{-c_{T0}\tau/z_0} + e^{-(2c_{T0}\tau)/z_0}\right] \tag{4.60}$$

$$\Omega_b^2(\tau) = \left(\frac{c_{T0}}{4H_0}\right)^2 \left[4\left(\frac{H_0}{z_0}\right)^2 + e^{-(2c_{T0}\tau)/z_0}\right] \tag{4.61}$$

We apply the Oscillation Theorem and obtain the turning point frequency just like the previous case explained in section 4.2.1.1. The turning point frequencies can be written using Equations (4.42-4.43)

$$\Omega_{tp,v}^2(\tau) = \Omega_v^2(\tau) + \frac{1}{4}\frac{1}{\tau^2}$$

$$\Omega_{tp,b}^2(\tau) = \Omega_b^2(\tau) + \frac{1}{4}\frac{1}{\tau^2}$$

Comparing (4.60) and (4.61) we can say that $\Omega_{tp,v}^2 > \Omega_{tp,b}^2$ and so

$\Omega_{cutoff} = \Omega_{tp,v}^{1/2}$, which in terms of ξ (using 4.52) is

$$\Omega_{cutoff}(\xi) = \Omega_0 \left[\frac{1}{\xi^2} + 8\left(\frac{H_0}{z_0}\right)\frac{1}{\xi} + 4\left(\frac{H_0}{z_0}\right)^2 \left(1 + \frac{1}{(\ln \xi)^2}\right)\right]^{1/2} \tag{4.62}$$

where $\Omega_0 \equiv \frac{c_{T0}}{4H_0}$.

4.2.3 Cutoff Frequency for General Case m > 2

Now we derive the cutoff frequencies for a general case and obtain general turning point frequency for all m. We begin by rewriting the general equations and obtain the critical frequency like the earlier sections. First we consider a general case of power law model for the temperature as follows,

$$T_0(\xi) = T_{00}\xi^m \tag{4.63}$$

$$c_s^2(\xi) = c_{S0}^2\xi^m \tag{4.64}$$

$$H(\xi) = H_0\xi^m \tag{4.65}$$

where $\xi = \frac{z}{z_0}$ and H_0 is a constant. Using Equations (4.8 – 4.10), we rewrite to get

$$\rho_0(\xi) = \rho_{00}\frac{1}{\xi^m} e^{\left[\frac{z_0}{(m-1)H_0\xi^{m-1}}\right]} \tag{4.66}$$

$$\rho_e(\xi) = \rho_{e0}\frac{1}{\xi^m} e^{\left[\frac{z_0}{(m-1)H_0\xi^{m-1}}\right]} \tag{4.67}$$

The horizontal gas pressure now becomes

$$B_0^2(\xi) = B_{00}^2 e^{\left[\frac{z_0}{H_0}\frac{1}{(m-1)\xi^{m-1}}\right]} \tag{4.68}$$

Then using Equations (4.66 – 4.68) we get

$$c_T^2(\xi) = c_{T0}^2 \xi^m \tag{4.69}$$

We can now calculate τ and ξ, and obtain

$$\tau = \left(\frac{2}{2-m}\right)\frac{z_0}{c_{T0}}\xi^{\left(\frac{2-m}{2}\right)} \tag{4.70}$$

$$\xi = \left[\left(\frac{|2-m|}{2}\right)\frac{c_{T0}}{z_0}\right]^{2/(2-m)} \tau^{\frac{2}{2-m}} \tag{4.71}$$

which allows us to derive expressions for, $c_T(\tau)$, $H(\tau)$ and their derivatives

$$c_T(\tau) = c_{T0}\left[\left(\frac{|2-m|}{2}\right)\frac{c_{T0}}{z_0}\right]^{m/(2-m)} \tau^{m/(2-m)} \tag{4.72}$$

$$H(\tau) = H_0\left[\left(\frac{|2-m|}{2}\right)\frac{c_{T0}}{z_0}\right]^{2m/(2-m)} \tau^{2m/(2-m)} \tag{4.73}$$

$$\frac{c_T^{'}}{c_T} = \left(\frac{m}{2-m}\right)\frac{1}{\tau} \tag{4.74}$$

$$\frac{c_T^{''}}{c_T} = \frac{2m(m-1)}{(2-m)^2}\frac{1}{\tau^2} \tag{4.75}$$

$$\frac{H^{'}}{H} = \left(\frac{2m}{2-m}\right)\frac{1}{\tau} \tag{4.76}$$

$$\frac{c_T}{H} = \frac{c_{T0}}{H_0}\left[\left(\frac{|2-m|}{2}\right)\frac{c_{T0}}{z_0}\right]^{-m/(2-m)} \tau^{-m/(2-m)} \tag{4.77}$$

Hence, we obtain the critical frequencies using Equations (4.20-4.21),

$$\Omega_0 \equiv \frac{c_{T0}}{4H_0} \tag{4.78}$$

$$\Omega_v^2(\tau)=\Omega_0^2\left[\left(\frac{|2-m|}{2}\right)\frac{c_{T0}}{z_0}\right]^{-2m/(2-m)}\tau^{-2m/(2-m)}+\Omega_0\left(\frac{2m}{2-m}\right)\left[\left(\frac{|2-m|}{2}\right)\frac{c_{T0}}{z_0}\right]^{-m/(2-m)}\tau^{-2/(2-m)}$$

$$+\frac{m}{4}\frac{(4-m)}{(2-m)^2}\frac{1}{\tau^2} \tag{4.79}$$

$$\Omega_b^2(\tau)=\Omega_0^2\left[\left(\frac{|2-m|}{2}\right)\frac{c_{T0}}{z_0}\right]^{-2m/(2-m)}\tau^{-2m/(2-m)}+\frac{m}{4}\frac{(3m-4)}{(2-m)^2}\frac{1}{\tau^2} \tag{4.80}$$

The next step is to perform the Fourier Transform of Equations (4.22 -4.23) in time and then apply the Oscillation Theorem to obtain the turning point frequencies (4.42-4.43). Substituting we get,

$$\Omega_{tp,v}^2(\tau)=\Omega_0^2\left[\left(\frac{|2-m|}{2}\right)\frac{c_{T0}}{z_0}\right]^{-2m/(2-m)}\tau^{-2m/(2-m)}+\Omega_0\left(\frac{2m}{2-m}\right)\left[\left(\frac{|2-m|}{2}\right)\frac{c_{T0}}{z_0}\right]^{-m/(2-m)}\tau^{-2/(2-m)}$$

$$+\frac{1}{(2-m)^2}\frac{1}{\tau^2} \tag{4.81}$$

Similarly we can also obtain for the magnetic field,

$$\Omega_{tp,b}^2(\tau)=\Omega_0^2\left[\left(\frac{|2-m|}{2}\right)\frac{c_{T0}}{z_0}\right]^{-2m/(2-m)}\tau^{-2m/(2-m)}+\left(\frac{m-1}{2-m}\right)^2\frac{1}{\tau^2} \tag{4.82}$$

Next we express the turning point frequencies in terms of τ by using Equation (4.70),

$$\Omega_{tp,v}^2(\xi)=\Omega_0^2\left[\xi^{-m}+4m\left(\frac{H_0}{z_0}\right)\xi^{-1}+4\left(\frac{H_0}{z_0}\right)^2\xi^{m-2}\right] \tag{4.83}$$

$$\Omega_{tp,b}^2(\xi)=\Omega_0^2\left[\xi^{-m}+4(m-1)^2\left(\frac{H_0}{z_0}\right)^2\xi^{m-2}\right] \tag{4.84}$$

They can also be written as

$$\Omega_{tp,v}^2(\xi) = 4\Omega_0^2\left(\frac{H_0}{z_0}\right)^2\left[\xi^{m-2} + m\left(\frac{z_0}{H_0}\right)\xi^{-1} + \frac{1}{4}\left(\frac{z_0}{H_0}\right)^2\xi^{-m}\right] \tag{4.85}$$

$$\Omega_{tp,b}^2(\xi) = 4\Omega_0^2\left(\frac{H_0}{z_0}\right)^2\left[(m-1)^2\xi^{m-2} + \frac{1}{4}\left(\frac{z_0}{H_0}\right)^2\xi^{-m}\right] \tag{4.86}$$

4.2.3.1 Determination of Cutoff Frequency

We can determine the cutoff frequency by determining the larger of the two frequencies derived above. We begin by considering the inequality $\Omega_{tp,b}^2/\Omega_0^2 > \Omega_{tp,v}^2/\Omega_0^2$ and use (4.83-4.84) to obtain,

$$(m-2)\xi^{m-1} > \left(\frac{z_0}{H_0}\right) \tag{4.87}$$

Since (m-2) is always larger than, or equal to, 1 and since ξ is also larger than 1; the left-hand-side of (4.87) is always larger than 1 and increases with height 'z' because $\xi = z/z_0$. Hence for $z_0 \le H_0$, the inequality (4.87) is always satisfied.

An interesting case is when $z_0 > H_0$; in which case, the right-hand-side may initially be larger than the right-hand-side, at least till the height where ξ^{m-1} becomes larger than z_0/H_0. However, when z_0/H_0 is fixed, ξ^{m-1} increases with height.

Thus the larger ($\Omega_{tp,b}^2/\Omega_0^2 > \Omega_{tp,v}^2/\Omega_0^2$) of the turning point frequencies gives the cutoff frequency, which from (4.83) is

$$\Omega_{cutoff}(\xi) = \Omega_0\left[\xi^{-m} + 4(m-1)^2\left(\frac{H_0}{z_0}\right)^2\xi^{m-2}\right]^{1/2} \tag{4.88}$$

4.3 Plots for Power Law Models

We now plot the cutoff frequencies and analyze the propagation of transverse tube waves. It is assumed that z_0 is the base of the tube and it corresponds to the location of the source for transverse tube waves. We consider two locations for this analysis,

Case 1: Wave Source at height, $z_0 = 10km$ and temperature, $T_{00} = 5000K$

Case 2: Wave Source at height, $z_0 = 50km$ and temperature, $T_{00} = 5500K$

The first plot shows the behavior of temperature for various power law models i.e., varying m in the relation $T = T_{00}\xi^m$ where $\xi = z/z_0$.

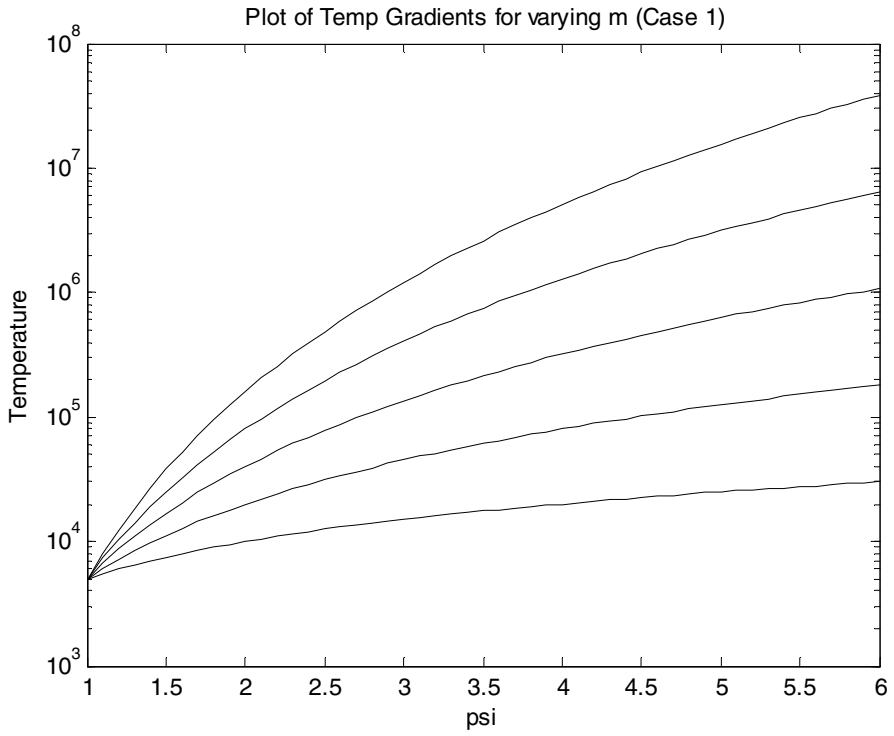

Figure 4.1 Plot of Temperature Gradients Vs Height for different values of m (m =1, 2, 3, 4, 5) for Case 1.

We can see that for increasing m, the temperature gradient becomes steeper. The same analysis is done for both the cases and the shape of the curves are similar for both cases.

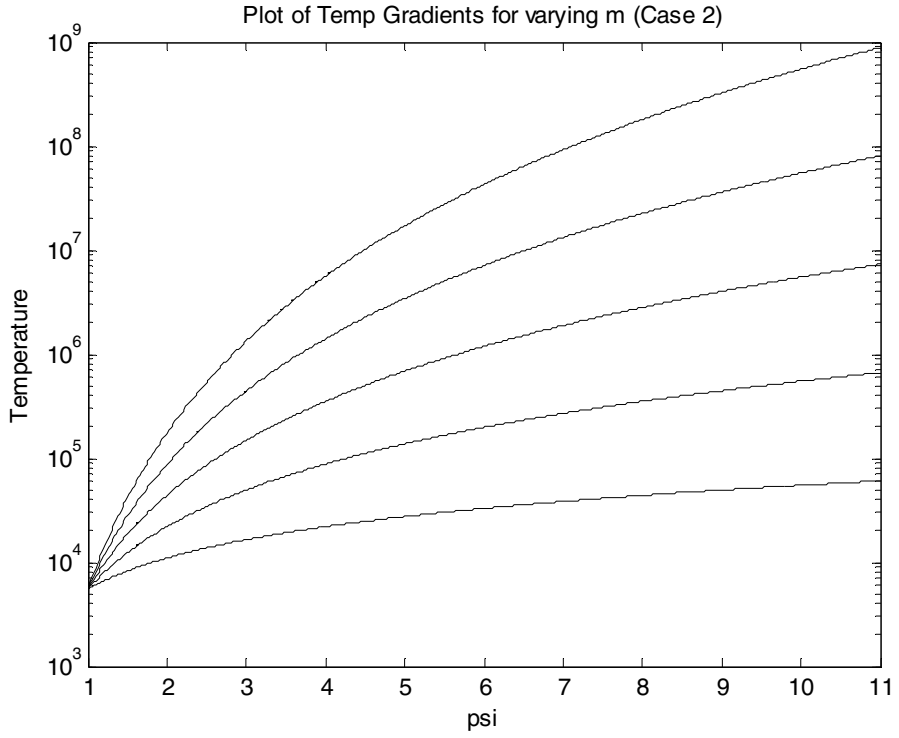

Figure 4.2 Plot of Temperature Gradients Vs Height for different values of m (m = 1, 2, 3, 4, 5) for Case 2.

Now, we plot the cutoff frequency for the case m = 1 and m = 2 using equations (4.46) and (4.62). We perform the analysis for both cases and find by looking at the plots that, if the wave has a frequency that is larger than the cutoff frequency at the height z_0, then the wave will propagate forever, as the cutoff frequency is seen to decrease with height. This behavior is characteristic for the non-isothermal models with

m = 1 and m = 2 as they correspond to the linear and parabolic temperature increase with height, respectively. The obtained results are shown in Figure 4.3 and Figure 4.4 given below.

Similarly we analyze the general case by plotting the turning point frequencies given by (4.83) and (4.84) for different values of m in the subsequent plots. The cutoff frequency is determined by choosing the larger of the turning point frequencies, which is the magnetic field for values of m>2.

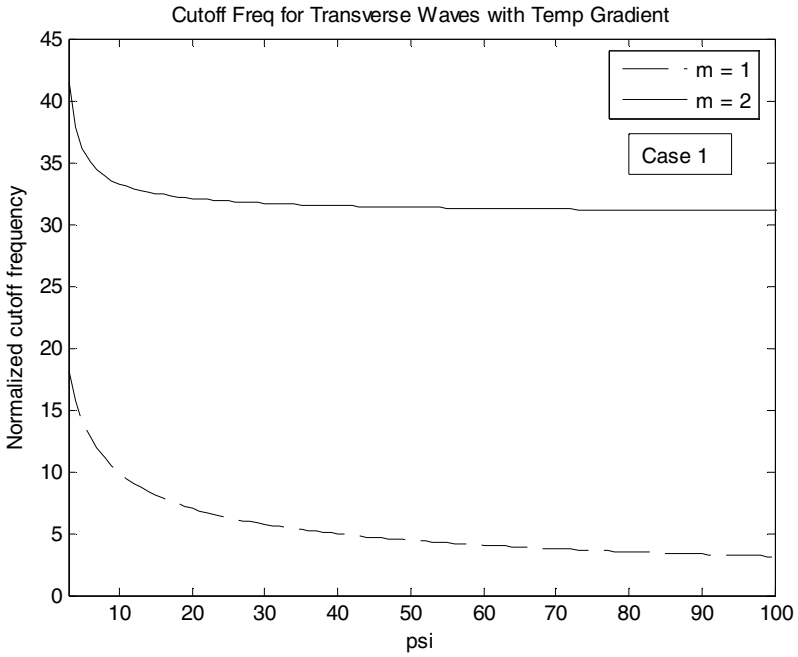

Figure 4.3 Cutoff frequency Vs Height for m = 1 and 2 for Case 1.

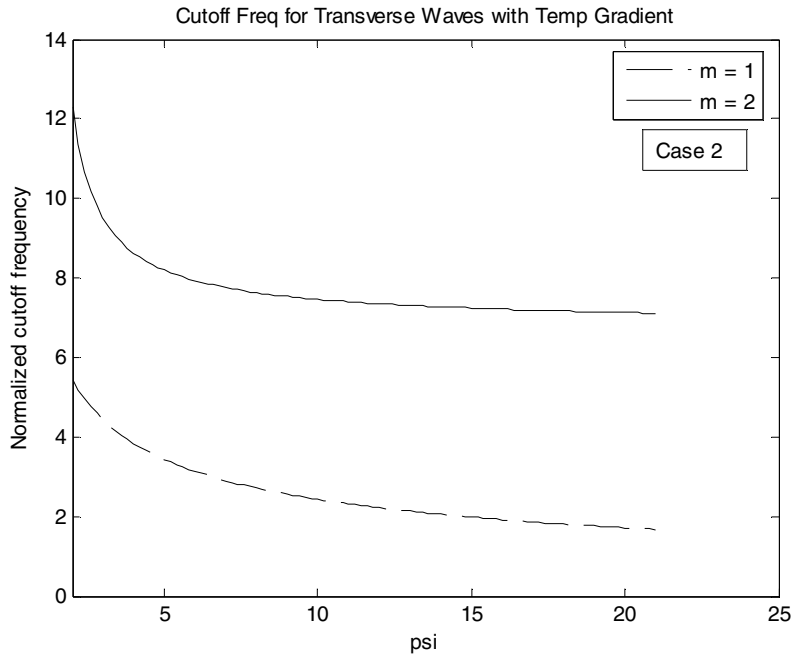

Figure 4.4 Cutoff frequency Vs Height for m = 1 and 2 for Case 2.

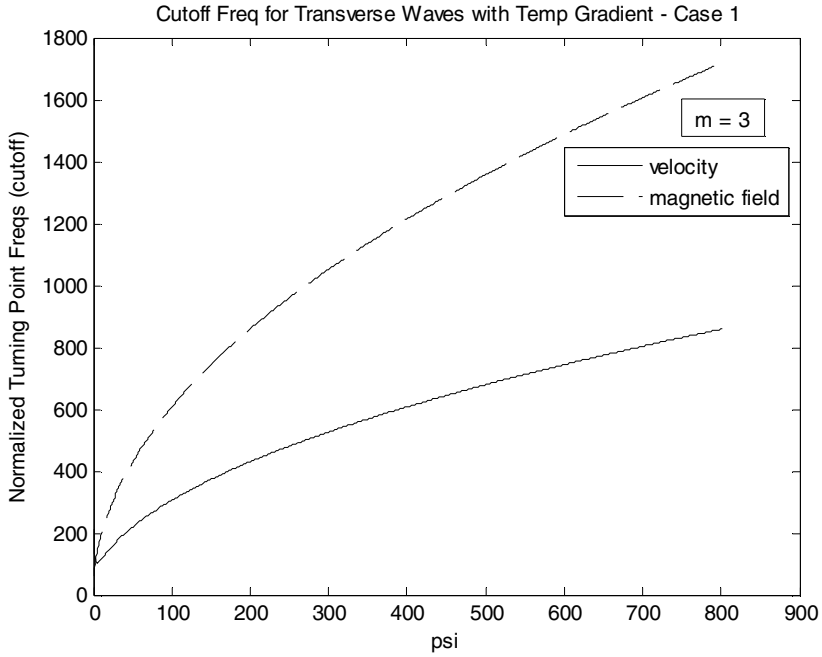

Figure 4.5 Cutoff frequency Vs Height for m = 3 for Case 1.

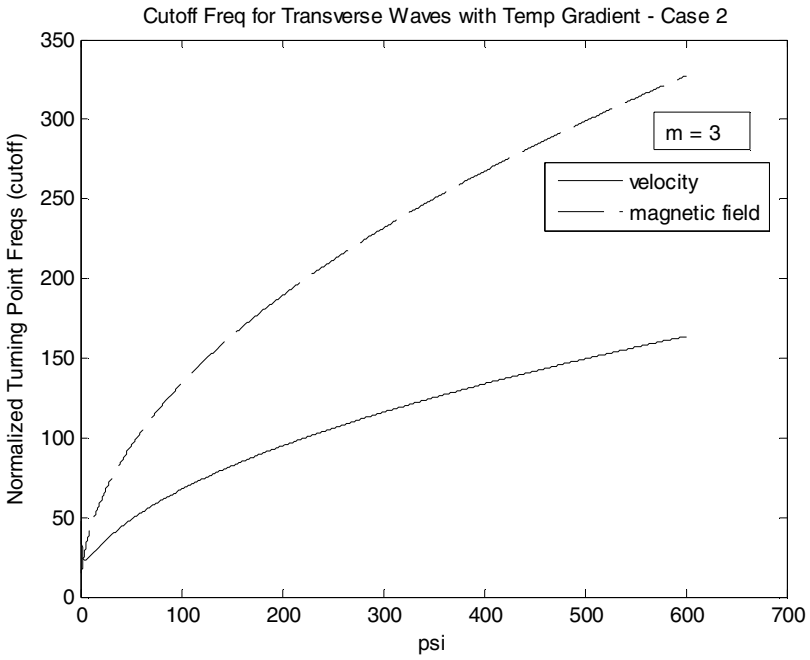

Figure 4.6 Cutoff frequency Vs Height for m = 3 for Case 2.

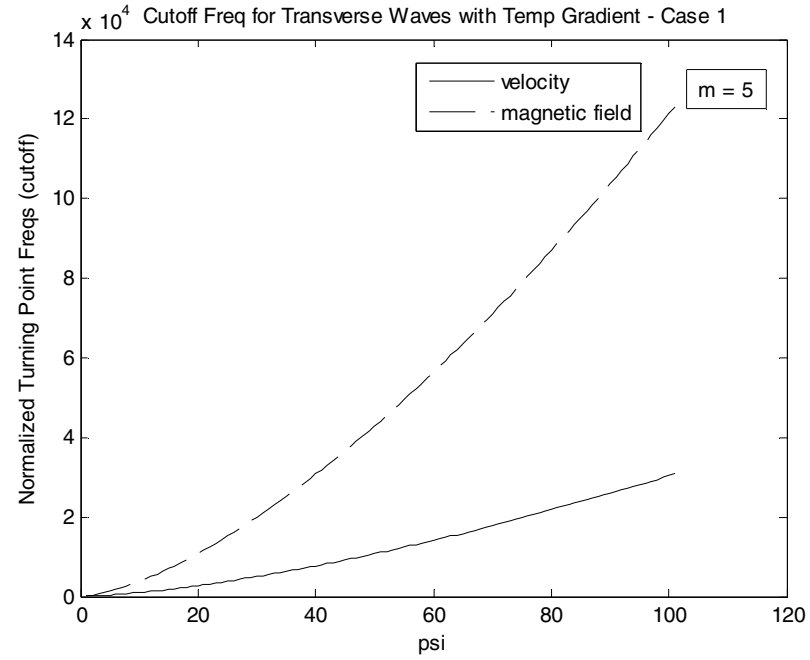

Figure 4.7 Cutoff frequency Vs Height for m = 5 for Case 1.

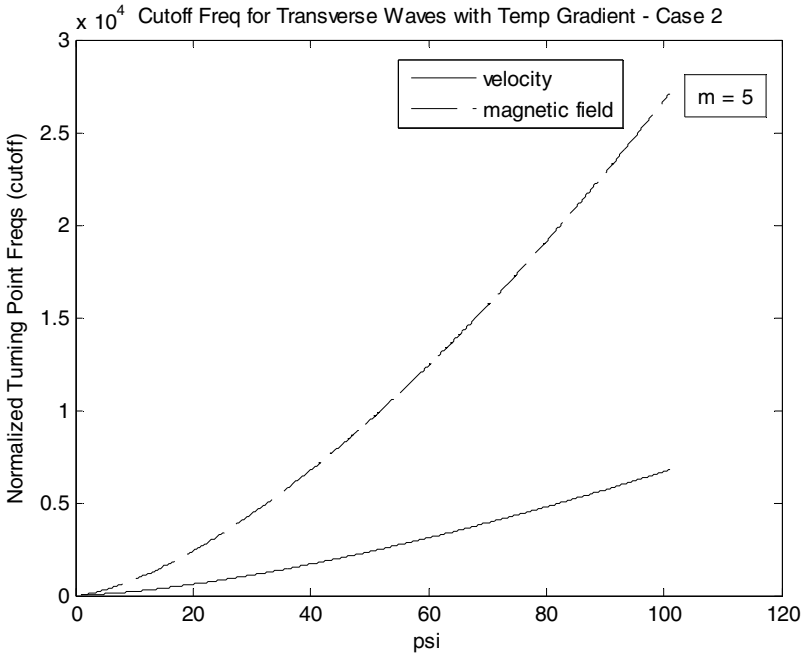

Figure 4.8 Cutoff frequency Vs Height for m = 5 for Case 2.

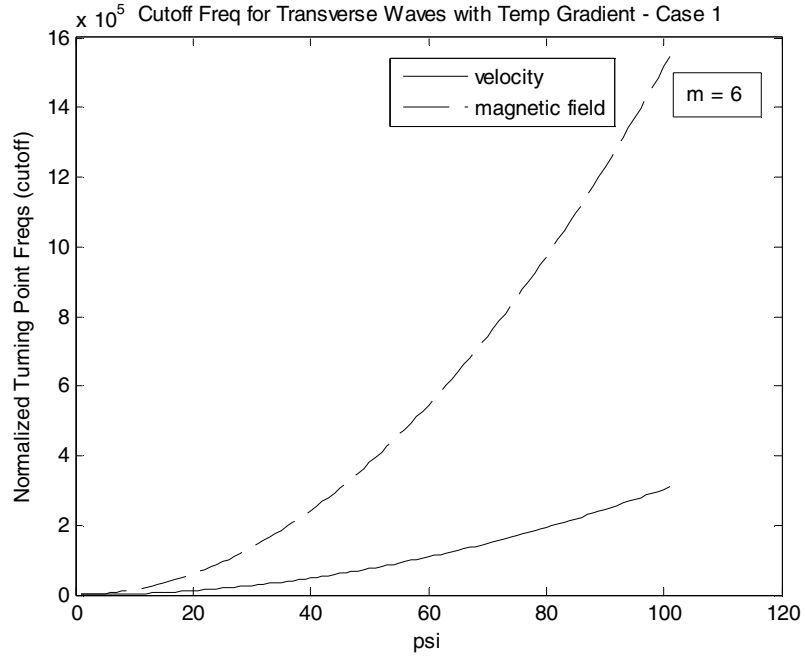

Figure 4.9 Cutoff frequency Vs Height for m = 6 for Case 1.

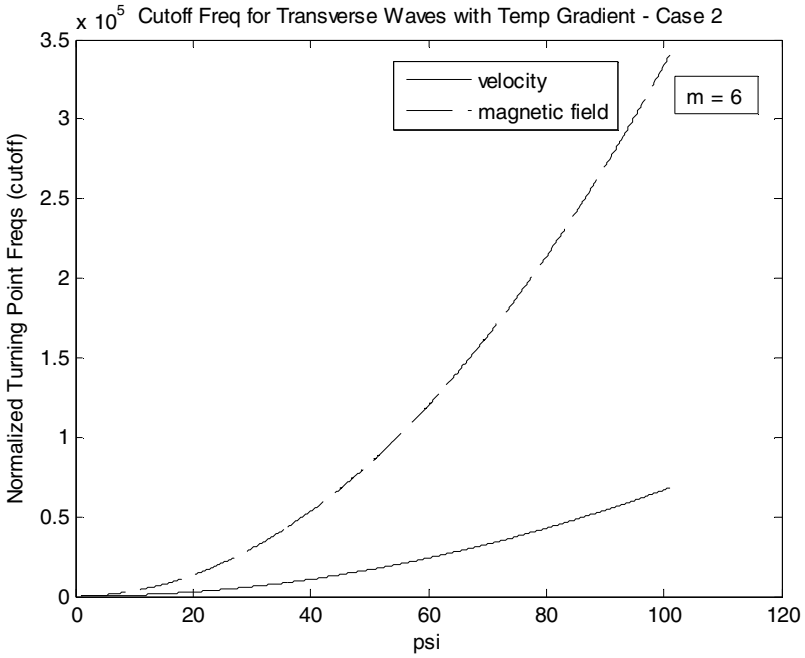

Figure 4.10 Cutoff frequency Vs Height for m = 6 for Case 2.

We can determine the cutoff frequency by choosing the larger of the two turning point frequencies given by (4.83) and (4.84). According to equation (4.87), the turning point frequency of the magnetic field component is larger than the velocity component and this is verified in the plots above (see Figures 4.5 – 4.10). By looking at the Figures, we see that the turning point frequencies are local quantities that sharply increase with height for the models with higher values of m, which correspond to steep temperature gradients.

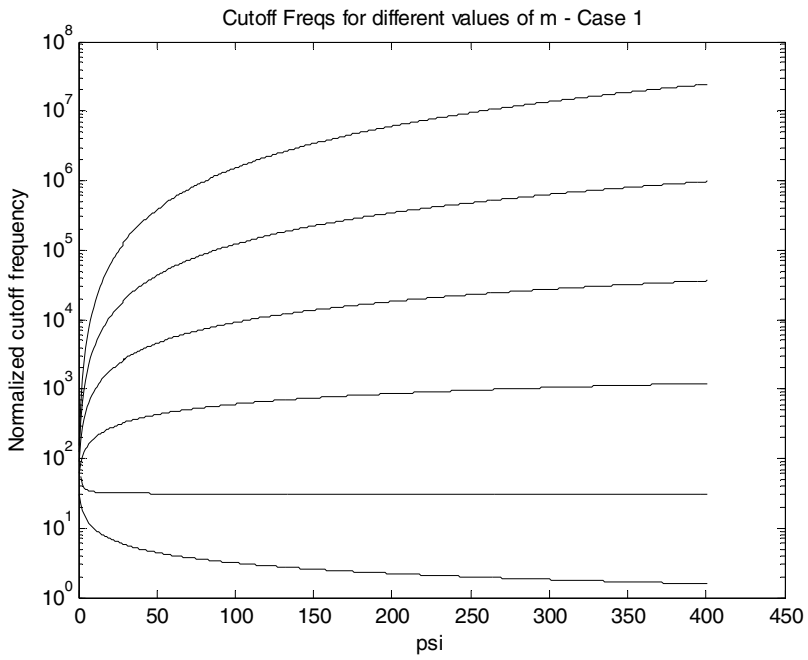

Figure 4.11 Plot of Normalized Cutoff frequencies Vs Height for different values of m (where m = 1, 2, 3, 4, 5, 6) for Case 1.

We then plot the cutoff frequency for different values of m. For this, we use a log scale for the normalized frequency and plot the cutoff frequency for both Case 1 and Case 2. Again, comparing Figure 4.11 and 4.12, we can see that shape of the curve is similar. We can conclude that as the value of m increases, the temperature gradient becomes steeper and the cutoff frequency also increases steeply.

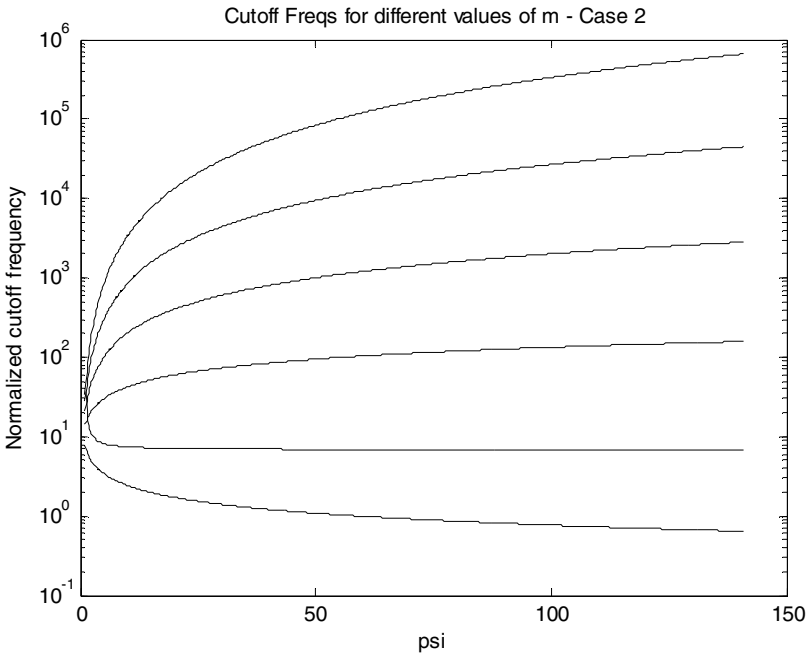

Figure 4.12 Plot of Normalized Cutoff frequencies Vs Height for different values of m (where m = 1, 2, 3, 4 ,5 ,6) for Case 2.

So for a wave to reach a certain height in a non-isothermal atmosphere, the wave source must generate waves with frequencies that are higher than the cutoff frequency corresponding to that height. For waves with frequencies lower than the cutoff at a given height, the atmosphere acts like a wall and reflects the waves. Hence, only those waves, whose frequency is higher than the cutoff, will propagate.

CHAPTER 5

SOLAR OSCILLATIONS

5.1 Introduction

The solar atmosphere is known to oscillate with periods that are different from those of the solar photosphere. While the latter is dominated by 5-min (p-mode) oscillations, the solar chromosphere oscillates with 3-min oscillations [4], [6]. Observations of Ca II H and K, Hα and the Ca II infrared triplet lines show that these chromospheric oscillations range from 2 to 5 min inside non-magnetic or weak magnetic regions like supergranulation cells. However the oscillations in the magnetic regions located at the boundaries of supergranules, which form the magnetic network, range from 6 to 15min [33], [7], [36], [17]. The solar p-mode and atmospheric oscillations in supergranulation cells and in the magnetic network are shown in the Figure 5.1 [45].

The 3 min period is usually interpreted as the acoustic cutoff period in the upper photosphere and these waves are observed at all heights in the cell interior. For example, they can be observed at the base of the chromosphere in the Mg II line; in the middle layers in the Ca II K line; in the upper layers of neutral C, N and O; and at the top of the chromosphere in the Lyman continuum [47].

Detection of oscillations in the solar transition region, coronal loops and coronal holes has provided evidence for the existence of waves in the upper regions of the solar

atmosphere. There is also increasing observational evidence that oscillations in the solar corona, transition region and chromosphere can be triggered by flares and other impulsive phenomena.

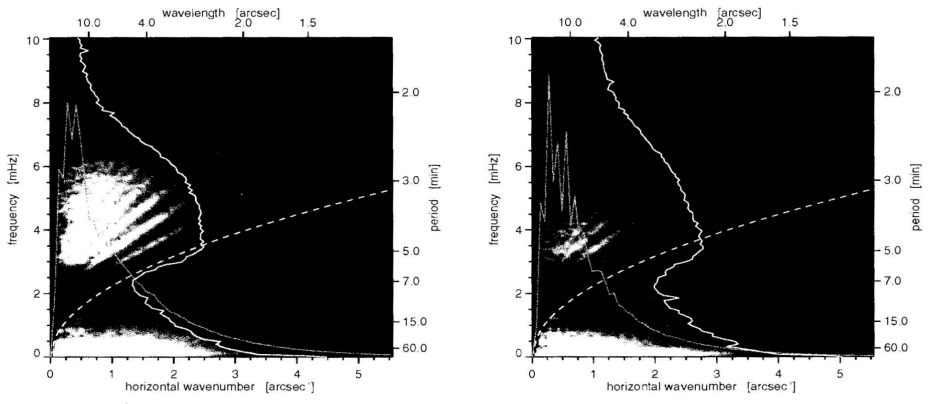

Figure 5.1 Observed 2-D brightness spectra of solar supergranulation cells (left) and magnetic network (right) [45].

5.2 Chromospheric Models

Many authors have attempted to describe the global parameters in the chromosphere using line ratios and emission measures. Chromospheric modeling is done by both empirical and semi-empirical techniques [50]. Empirical methods have been used to determine the mean temperature and density in the chromosphere by measuring the integrated flux of lines formed in the chromosphere. Semi-empirical methods are used to obtain detailed information in the chromosphere. We know that the chromosphere is at a temperature greater than the effective temperature i.e.,

$\langle T_{chromosphere} \rangle > \langle T_{photosphere} \rangle$. This is incorporated in the synthetic spectra till it matches the observed spectra [50]. Spectroheliograms of chromospheric lines (Ca II H and K) show the solar chromosphere to be vertically and horizontally inhomogeneous.

5.3 VAL Model

The most used chromospheric model is that of Vernazza, Avrett, and Loeser (VAL). The VAL model is a useful one-dimensional semi-empirical model which is characterized by rising temperature that is carefully chosen to reproduce the chromospheric emission observed in many spectral lines [46], [48]. In the models presented in these papers, Model C of VAL III gives synthetic spectra that best reproduce the solar spectrum in the near-UV, Visible, IR and microwave for the non-active regions (quiet regions outside the magnetically active region) [48], [50].

5.3.1 Constructing a Magnetic Flux Tube from the VAL Model

We begin with the VAL model C and rescale the height. Then we calculate the sound speed for each height using the relation

$$c_s^2(z) = \frac{\gamma(z) p(z)}{\rho(z)}$$

We take, the height (z) dependent, values from the model. Then we determine the new scale height using

$$H(z) = \frac{c_s^2(z)}{\gamma(z) g}$$

Then we perform numerical integration to obtain the value of the magnetic field using,

$$B_0 = B_{00} e^{-\frac{1}{2}\int_0^z \frac{d\tilde{z}}{H(z)}}$$

where, we take H(z) from the above calculations and assume $B_{00} = 1500G$. Then we determine the pressure inside the tube using the horizontal pressure balance equation,

$$p_0(z) = p_e(z) - \frac{B_0^2(z)}{8\pi}$$

Where p_0 is the pressure inside the magnetic flux tube and p_0 is the pressure outside. The final parameter to calculate is the density inside the tube, given by,

$$\rho_0(z) = \frac{\gamma p_0(z)}{c_s^2(z)}$$

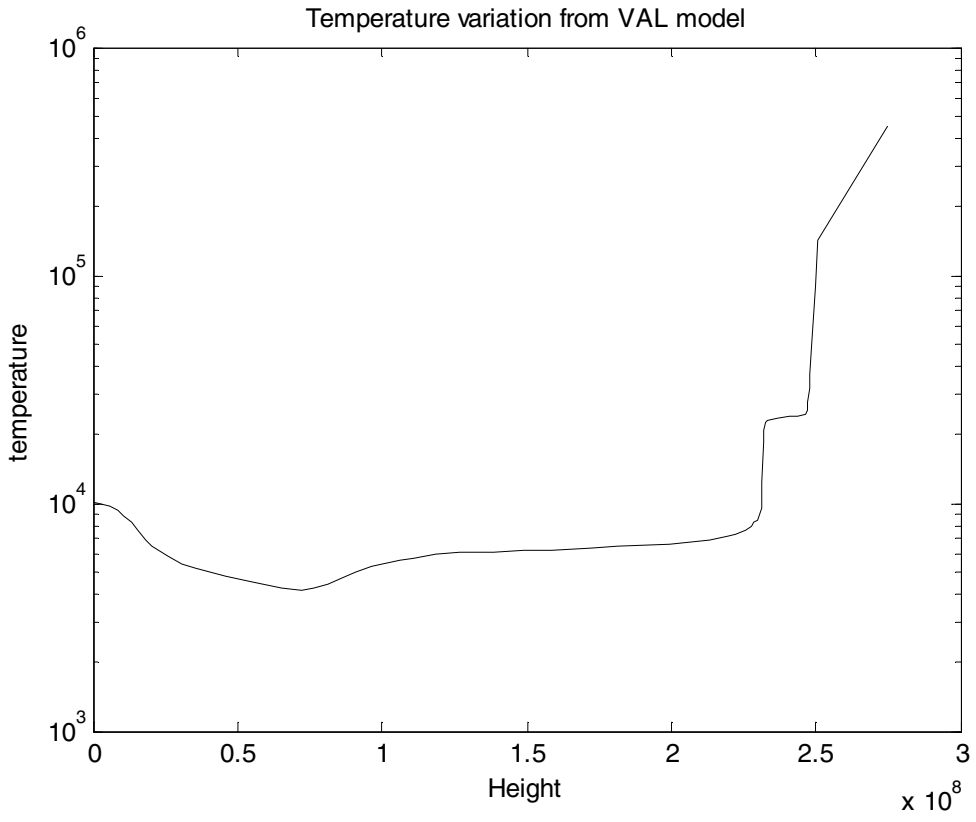

Figure 5.2 Plot of temperature variation with height from the VAL C Model.

5.3.2 Cutoff Frequency from the VAL Model

Next we determine the cutoff frequency for transverse tube waves propagating in the magnetic flux tube constructed from the VAL Model. We determine other tube parameters using the equations from Chapter 4, and

$$c_T^2 \equiv \frac{B_0^2}{4\pi(\rho_0 + \rho_e)}$$

A plot of the transverse tube velocity, c_T and sound speed, c_S (Figure 5.3) reveals that although their distribution with height are very similar and resemble the VAL temperature variation (Figure 5.2), c_T is seen to be lower than c_S. Hence we can conclude that these distributions are caused by the solar temperature gradients as otherwise, both are found to be constant in an isothermal atmosphere.

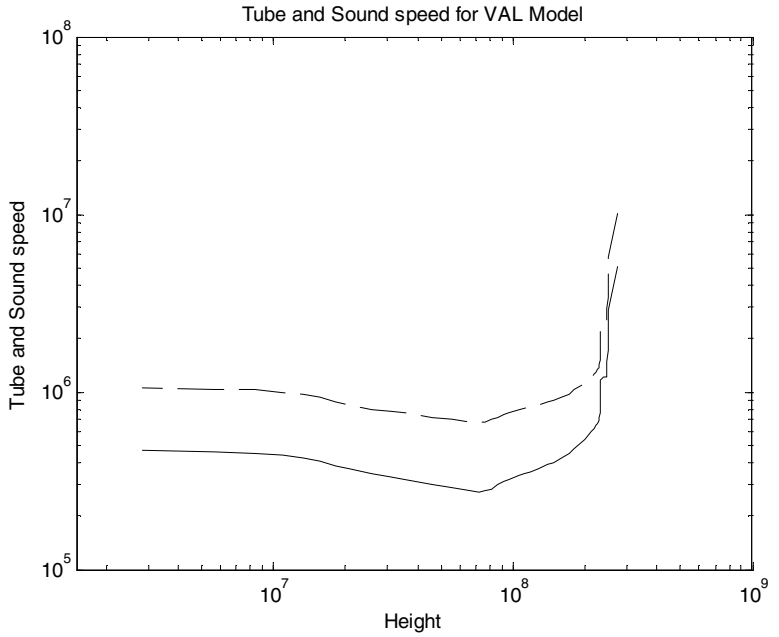

Figure 5.3 Plot of transverse tube (solid line) and sound speed (dotted line) with temperature gradient for the VAL C Model.

$$d\tau = \frac{dz}{c_T}$$

We calculate τ by numerical integration for each height given by the VAL Model. Then, we can calculate the critical frequencies by using,

$$\Omega_v^2(\tau) = \frac{c_T^2}{16H^2} + \frac{3}{4}\left(\frac{c_T'}{c_T}\right)^2 + \frac{1}{4}\frac{c_T H'}{H^2} - \frac{1}{2}\frac{c_T''}{c_T}$$

$$\Omega_b^2(\tau) = \frac{c_T^2}{16H^2} - \frac{1}{4}\left(\frac{c_T'}{c_T}\right)^2 - \frac{1}{4}\frac{c_T H'}{H^2} + \frac{1}{2}\frac{c_T''}{c_T} + \frac{1}{2}\frac{c_T'}{H}$$

and determine the turning point frequency using,

$$\Omega_{tp,v}^2(\tau) = \Omega_v^2(\tau) + \frac{1}{4}\frac{1}{\tau^2}$$

$$\Omega_{tp,b}^2(\tau) = \Omega_b^2(\tau) + \frac{1}{4}\frac{1}{\tau^2}$$

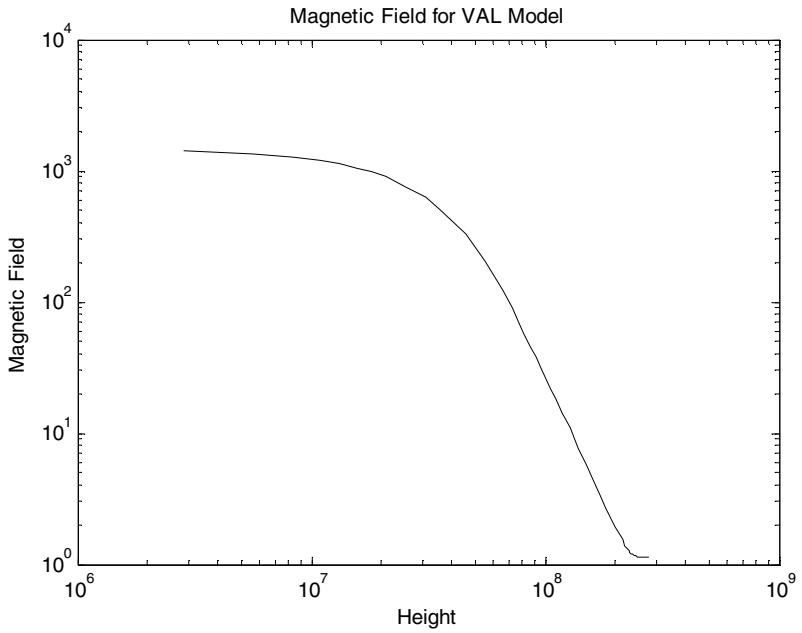

Figure 5.4 Variation of Magnetic Field with height.

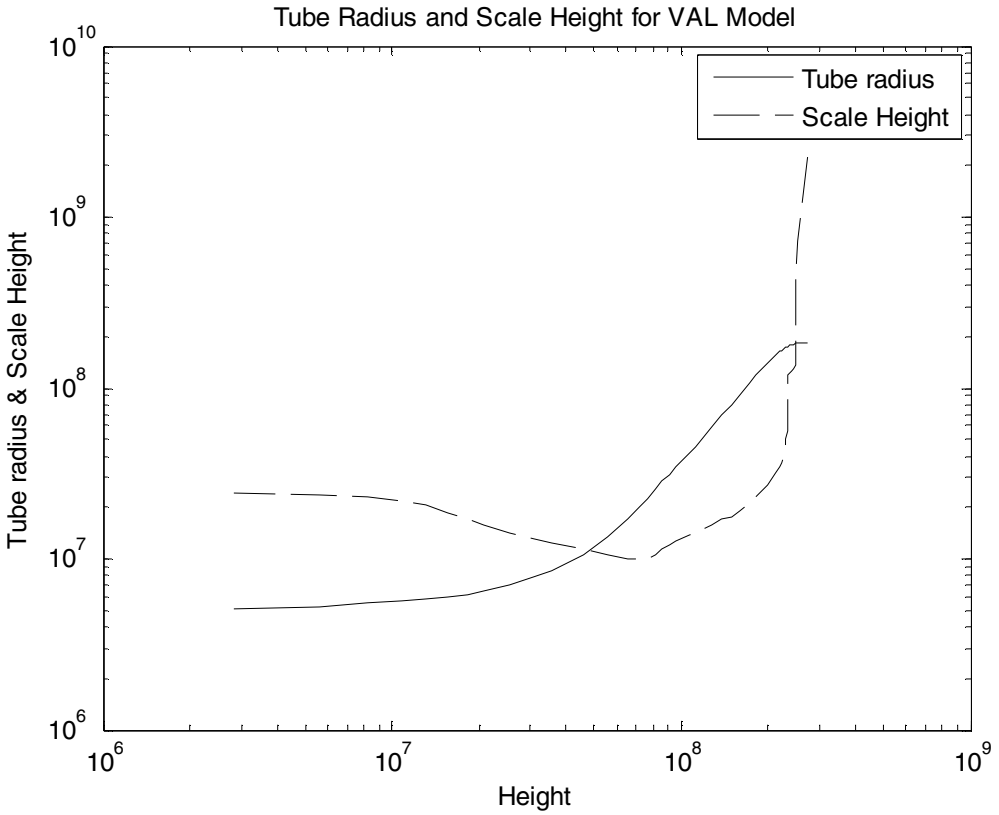

Figure 5.5 Plot of tube radius (solid line) and scale height (dotted line).

A plot of the magnetic field with height is shown in Figure 5.4, which shows that the field decreases exponentially with height. We can also compare the tube radius and the scale height, to determine the region where the thin flux tube assumption is valid. As seen from Figure 5.5, when the scale height exceeds the tube radius, the assumption of thin flux tube is no longer valid.

We then plot the cutoff frequency which is the larger of the turning point frequencies. Figure 5.6 shows the cutoff for the entire model.

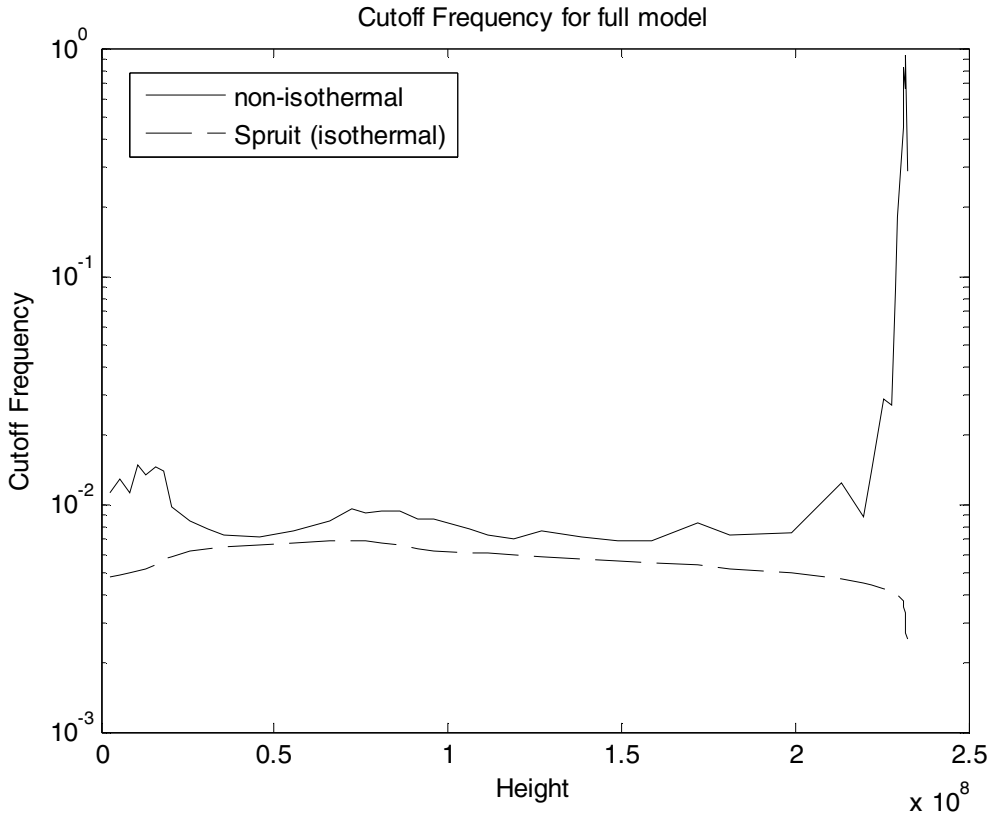

Figure 5.6 Plot of cutoff frequency and Spruit frequency with temperature gradient for the VAL C Model.

The obtained results demonstrate that the effects of the temperature gradient on the cutoff frequency for transverse waves propagating along a thin magnetic flux tube embedded in the VAL model are the most important in the upper layers of the solar photosphere and the lower layers of the solar chromosphere. The main result of this thesis is that the cutoff frequency calculated here exceeds that derived by Spruit [42] for an isothermal atmosphere by a factor of 3 at the base of the VAL model. However, the cutoffs (see Figure 5.7) become comparable in those regions of the solar chromosphere

where the thin flux tube approximation breaks down (see Figure 5.5 for this break down).

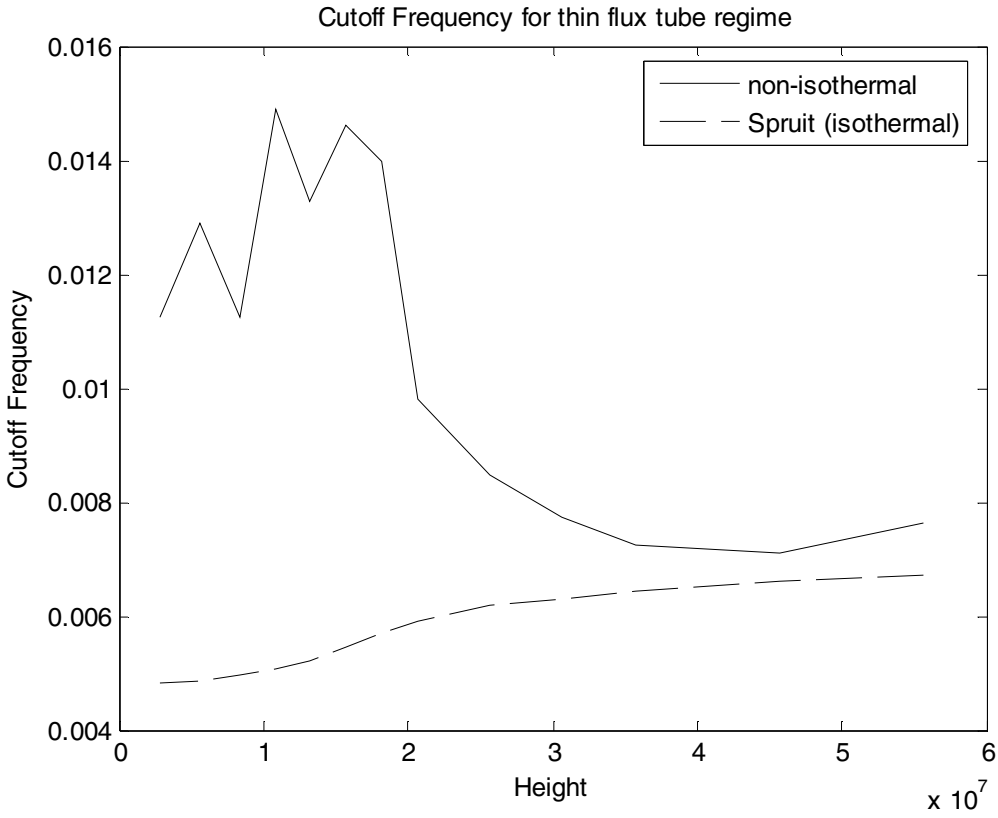

Figure 5.7 Plot of cutoff frequency and Spruit frequency with temperature gradient for the thin flux tube approximation.

The difference between the cutoff frequency calculated here and that obtained by Spruit in the solar photosphere will be important for the energy carried by transverse tube waves from the solar convection zone, where the waves are generated, to the overlying solar atmosphere, where the wave energy is deposited.

In the middle of the solar atmosphere, where 7 min chromospheric oscillations are observed, there is agreement between the two cutoffs, so the obtained results do not have significant effects on the oscillations.

Extension of our analytical treatment to the entire VAL model shows that there is significant discrepancy between the cutoff derived here and Spruit's cutoff; however, it must be kept in mind that this extension is beyond the thin flux tube limit used in our derivations of the cutoff frequency.

CHAPTER 6

CONCLUSION

The effects of temperature gradients on transverse tube waves were studied analytically with power law models in Chapter 4. The cutoff becomes a local quantity in a non-isothermal atmosphere and its physical meaning is different from that observed as global cutoff for isothermal atmosphere.

For the temperature gradient which corresponds to m = 1 and m = 2, it was observed that the turning point frequencies corresponding to the velocity perturbations are larger and hence they are chosen to become the cutoff frequencies. It was also observed that these cutoffs decrease with height and so waves whose frequencies are higher than the cutoff frequencies will propagate forever.

While considering non-isothermal models with m >2, it was found that the turning point frequencies corresponding to the magnetic field perturbations are larger, so they were chosen as the cutoff frequencies for these models. It was observed that as m was increased, the cutoff frequency also sharply increased. So in order for a transverse tube wave to reach a certain height, the wave source at the base must excite waves that have frequencies higher than the cutoff frequency at that height. Otherwise, the waves will be reflected.

Extension of our analytical treatment to the entire VAL model shows that there is significant discrepancy between the cutoff derived here and Spruit's cutoff; however,

it must be kept in mind that this extension is beyond the thin flux tube limit used in our derivations of the cutoff frequency. The difference between the cutoff frequency calculated here and that obtained by Spruit in the solar photosphere will be important for the energy carried by transverse tube waves from the solar convection zone, where the waves are generated, to the overlying solar atmosphere, where the wave energy is deposited.

The obtained results demonstrate that the effects of the temperature gradient on the cutoff frequency for transverse waves propagating along a thin magnetic flux tube embedded in the VAL model are the most important in the upper layers of the solar photosphere and the lower layers of the solar chromosphere. The main result of this thesis is that the cutoff frequency calculated here exceeds that derived by Spruit [42] for an isothermal atmosphere by a factor of 3 at the base of the VAL model, where the thin flux tube approximation is valid.

APPENDIX A

OSCILLATION AND TURNING POINT THEOREMS

Oscillation Theorem

Consider an ordinary differential equation of the form,

$$\frac{d^2\phi}{dx^2} + \Phi(x)\phi = 0$$

which is known to have all its solutions to be periodic. Assume that there is another equation of the form,

$$\frac{d^2\psi}{dx^2} + \Psi(x)\psi = 0$$

where $\Psi(x) > \Phi(x)$ for all x. Then, all of the solutions of the above equation are also periodic. The proof of this theorem is given in literature [16].

Turning Point Theorem

Consider an ordinary differential equation of the form

$$\frac{d^2\phi}{dx^2} + \Phi(x)\phi = 0$$

which is known to have a turning point that separates the periodic and non periodic solutions. Assume that there is another equation of the form

$$\frac{d^2\psi}{dx^2} + \Psi(x)\psi = 0$$

This equation has a turning point only if the condition, $\Psi(x) = \Phi(x)$ is satisfied for all x.

APPENDIX B

EULER'S EQUATION AND ITS TURNING POINT

In general, Euler's equation can be written in the following form [25]:

$$\frac{d^2y}{dx^2} + \frac{C_E}{4x^2}\, y = 0$$

where C_E is a constant whose value determines the form of the solution. For C_E >1, the equation has periodic solutions, however, the solutions become non-periodic when C_E <1, and finally for C_E = 1, there is a turning point, which separates these two distinct types of solutions.

A general form of the steady-state Klein-Gordon equation [27] is

$$\frac{d^2Y_i}{dx^2} + \left(\omega^2 - \Omega_i^2\right) Y_i = 0$$

where the form of the critical frequencies Ω_i^2 (x), with i = 1,2 and 3, may be different for different wave variables and for different models.

Using the oscillation theorem (see Appendix A), we show that the Klein-Gordon equation has periodic wave solutions when $\left[\omega^2 - \Omega_i^2(x)\right] > 1/4x^2$ is valid for all x. We use the turning point theorem (see Appendix A)to show that the Klein-Gordon has a turning point, if and only if, the condition $\left[\omega^2 - \Omega_i^2(x)\right] = 1/4x^2$ is valid for all x.

APPENDIX C

VAL C MODEL

VAL MODEL C modified at great depth similar to Bohn's convection model
A,T (temp),P (pressure),R (density),GAM

1	-2.5430E+08	4.4700E+05	1.4400E-01	2.3490E-15	1.6667E+00
2	-2.2980E+08	1.4100E+05	1.4700E-01	7.4940E-15	1.6667E+00
3	-2.2900E+08	8.9100E+04	1.4720E-01	1.1790E-14	1.6667E+00
4	-2.2800E+08	5.0000E+04	1.4770E-01	2.1130E-14	1.6667E+00
5	-2.2740E+08	3.7000E+04	1.4810E-01	2.8080E-14	1.6667E+00
6	-2.2710E+08	3.2000E+04	1.4830E-01	3.2220E-14	1.6667E+00
7	-2.2670E+08	2.8000E+04	1.4870E-01	3.6650E-14	1.6667E+00
8	-2.2630E+08	2.5500E+04	1.4910E-01	4.0170E-14	1.6667E+00
9	-2.2550E+08	2.4500E+04	1.5000E-01	4.2030E-14	1.6667E+00
10	-2.2300E+08	2.4200E+04	1.5300E-01	4.3550E-14	1.6667E+00
11	-2.2000E+08	2.4000E+04	1.5660E-01	4.5170E-14	1.6667E+00
12	-2.1600E+08	2.3500E+04	1.6170E-01	4.7950E-14	1.6667E+00
13	-2.1290E+08	2.3000E+04	1.6590E-01	5.0580E-14	1.6667E+00
14	-2.1200E+08	2.2500E+04	1.6720E-01	5.2160E-14	1.6667E+00
15	-2.1150E+08	2.1000E+04	1.6790E-01	5.6190E-14	1.6667E+00
16	-2.1130E+08	1.8500E+04	1.6820E-01	6.3900E-14	1.6667E+00
17	-2.1090E+08	1.2300E+04	1.6910E-01	9.5690E-14	1.6667E+00
18	-2.1070E+08	1.0700E+04	1.6970E-01	1.0930E-13	1.6667E+00
19	-2.1040E+08	9.5000E+03	1.7060E-01	1.2250E-13	1.6667E+00
20	-2.0900E+08	8.4400E+03	1.7580E-01	1.4330E-13	1.6667E+00
21	-2.0800E+08	8.1800E+03	1.7980E-01	1.5300E-13	1.6667E+00
22	-2.0700E+08	7.9400E+03	1.8420E-01	1.6280E-13	1.6667E+00
23	-2.0500E+08	7.6600E+03	1.9360E-01	1.8020E-13	1.6667E+00
24	-2.0160E+08	7.3600E+03	2.1180E-01	2.1220E-13	1.6667E+00
25	-1.9900E+08	7.1600E+03	2.2800E-01	2.4170E-13	1.6667E+00
26	-1.9250E+08	6.9400E+03	2.7800E-01	3.2270E-13	1.6667E+00
27	-1.7850E+08	6.6300E+03	4.5110E-01	6.0820E-13	1.6667E+00
28	-1.6050E+08	6.4400E+03	9.3340E-01	1.4930E-12	1.6667E+00
29	-1.5150E+08	6.3700E+03	1.4090E+00	2.4500E-12	1.6667E+00
30	-1.3800E+08	6.2800E+03	2.7740E+00	5.3150E-12	1.6667E+00
31	-1.2800E+08	6.2200E+03	4.7860E+00	9.8220E-12	1.6667E+00
32	-1.1800E+08	6.1500E+03	8.5270E+00	1.8390E-11	1.6667E+00
33	-1.0650E+08	6.0400E+03	1.7260E+01	4.0000E-11	1.6667E+00
34	-9.8000E+07	5.9250E+03	3.0080E+01	7.3590E-11	1.6667E+00
35	-9.0500E+07	5.7550E+03	5.0430E+01	1.2970E-10	1.6667E+00
36	-8.5500E+07	5.6500E+03	7.2100E+01	1.9020E-10	1.6667E+00
37	-7.5500E+07	5.2800E+03	1.5280E+02	4.3580E-10	1.6667E+00
38	-7.0500E+07	5.0300E+03	2.2830E+02	6.8640E-10	1.6667E+00
39	-6.5500E+07	4.7300E+03	3.4950E+02	1.1210E-09	1.6667E+00
40	-6.0500E+07	4.4200E+03	5.5160E+02	1.8990E-09	1.6667E+00

41	-5.5500E+07	4.2300E+03	8.9580E+02	3.2320E-09	1.6667E+00
42	-5.1500E+07	4.1700E+03	1.3360E+03	4.9020E-09	1.6667E+00
43	-4.5000E+07	4.2200E+03	2.5690E+03	9.3270E-09	1.6667E+00
44	-3.5000E+07	4.4650E+03	6.7980E+03	2.3340E-08	1.6667E+00
45	-2.5000E+07	4.7800E+03	1.6910E+04	5.4130E-08	1.6667E+00
46	-1.5000E+07	5.1800E+03	3.9260E+04	1.1500E-07	1.6667E+00
47	-1.0000E+07	5.4550E+03	5.8040E+04	1.6060E-07	1.6667E+00
48	-5.0000E+06	5.8400E+03	8.2740E+04	2.1520E-07	1.6667E+00
49	0.0000E+00	6.4200E+03	1.1720E+05	2.7270E-07	1.6667E+00
50	2.5000E+06	6.9100E+03	1.3680E+05	2.9490E-07	1.6667E+00
51	5.0000E+06	7.6100E+03	1.5750E+05	3.0800E-07	1.6667E+00
52	7.5000E+06	8.3200E+03	1.7900E+05	3.1920E-07	1.6667E+00
53	9.7894E+06	8.8150E+03	1.9950E+05	3.3578E-07	1.6667E+00
54	1.2362E+07	9.2750E+03	2.2390E+05	3.5816E-07	1.6667E+00
55	1.5043E+07	9.6200E+03	2.5120E+05	3.8742E-07	1.6667E+00
56	1.7812E+07	9.9100E+03	2.8180E+05	4.2189E-07	1.6667E+00
57	2.0665E+07	1.0170E+04	3.1620E+05	4.6129E-07	1.6667E+00

REFERENCES

[1] Abramowitz M., Stegun I.A., 1980, Handbook of Mathematical Functions. Dover Publications, New York, p.364

[2] Babcock H.W., 1963, In: Annual Review of Astronomy & Astrophysics, Vol 1, p. 41

[3] Chaisson E., McMillan S., 2002, Astronomy Today. Prentice Hall, New Jersey, p. 407

[4] Christensen-Dalsgaard, J., et al., 1996, Science, 272, 1286

[5] Curdt W., Heinzel P., 1998, Astrophysical Journal, p.503, L95

[6] De Pontieu, B., Erdelyi, R., & De Moortel, I., 2005, Astrophysical Journal, 624, L61

[7] Deubner, F.L., 1991, in "Mechanisms of Chromospheric and Coronal Heating", P. Ulmschneider, E. Priest and R. Rosner (Eds.), Berlin, Springer, p. 6

[8] Defouw R.J., 1976, Astrophysical Journal, p.209, 266

[9] Elmore W.C., Heald M.A., 1985, Physics of Waves. Dover Publications, New York, p.248

[10] Foukal P., 1990, Solar Astrophysics, John Wiley & Sons

[11] Friedberg J. P., 1987, Ideal Magnetohydrodynamics. Plenum Press, New York, p. 7-11

[12] Friedrichs K.O., 1954, In: Nonlinear Wave Motion in Magnetohydrodynamics. Los Alamos Report. LAMS-2105 (Physics)

[13] Huang P., Musielak Z.E., Ulmschneider P., 1995, Astronomy & Astrophysics 279, 579

[14] Ida N., Bastos J. P.A., 1992, Electromagnetics and Calculation of Fields. Springer-Verlag, New York, p. 28-33

[15] Jackson J. D., 1975, Classical Electrodynamics. John Wiley & Sons, Inc., New York, p. 485-489

[16] Kahn P. B., 1990, Mathematical Methods for Scientists and Engineers. John Wiley & Sons, p. 208

[17] Kalkofen, W., 1997, Astrophysical Journal, 486, L 145

[18] Kalkofen W., Rossi P., Bodo G., Massaglia S., 1994, Astronomy & Astrophysics 284, 976

[19] Kantrowitz and Petschek, 1963, Plasma Physics in Theory and Application: MHD Characteristics and Shock waves, p. 156-159

[20] Kulsrud R.M., 2005, Plasma Physics for Astrophysics, Princeton University Press, New Jersey

[21] Lamb H., 1908, Proc. Lond. Math. Soc., Ser 2, 7, 122

[22] Lamb H., 1932, Hydrodynamics. Dover Publications, New York

[23] Leighton, R., Noyes, R., & Simon, G.W., 1962, Astrophysical Journal , 135, 474

[24] Morse P.M., Feshbach H., 1953, Methods of Theoretical Physics, McGraw Hill, New York

[25] Murphy G. M., 1960, Ordinary Differential Equations and their Solutions, D. Van Nostrand Company, New York

[26] Musielak Z. E., Ulmschneider P., 2003, Astronomy & Astrophysics

[27] Musielak Z.E., Fontenla J. M., Moore R. L., 1992, Phys. Fluids B p 4, 13

[28] Musielak Z.E., Musielak D.E., Mobashi H., 2006, Physical Review p 0366121 -03661210

[29] Musielak Z.E., Routh S., Hammer R., 2006, Astronomy & Astrophysics

[30] Musielak Z.E., Ulmschneider P., 2003, Astronomy & Astrophysics

[31] Musielak Z.E., Ulmschneider P., 2001, Astronomy & Astrophysics, p. 541-554

[32] Musielak Z.E., Rosner R., Ulmschneider P., 1989, Astrophysical Journal, p. 337, 470

[33] Orrall, F.Q., 1966, Astrophysical Journal, 143, 917

[34] Roberts B., Ulmschneider P., 1998, Dynamics of Flux Tubes in the Solar Atmosphere: Theory In Lecture Notes in Physics. Springer-Verlag, Heidelberg Vol 489, p. 3,4

[35] Roberts B., Ulmschneider P., 1997, Solar & Heliospheric Plasma Physics, Springer-Verlag, Berlin, p. 75

[36] Rutten, R.G.M., & Uitenbroek, H., 1991, Solar Physics., 134, 15

[37] Schmitz F., Fleck B., 1998, Astronomy & Astrophysics, p 337, 487

[38] Spruit H.C., 1981, Astronomy & Astrophysics 129

[39] Spruit H. C., 1981, In: Solar Phenomena in Stars and Stellar Systems. D. Reidel Publishing Company, Boston, p. 289- 291

[40] Spruit H. C., Roberts B., 1983, Nature, p. 304, 401

[41] Spruit H.C., 1980, Astronomy & Astrophysics, p. 155

[42] Spruit H. C., 1982, In: Solar Physics. D. Reidel Publishing Company, Boston, p. 3, 8, 9, 13, 16

[43] Sutmann G., Musielak Z. E., Ulmschneider P., 1998, Astronomy & Astrophysics

[44] Sutmann G., Ulmschneider P., 1995, Astronomy & Astrophysics, p 294, 232

[45] Tritschler A., Schmidt., W., & Wedemeyer, S., 2005, A&A, submitted

[46] Ulmschneider P., Rammacher W., Musielak Z. E., Kalkofen W., 2005, The Astrophysical Journal, p L155-L158

[47] Vernazza J. E., Avrett E. H., Loeser R., 1981, Astrophysical Journal

[48] Wilhelm K. & Kalkofen, W. 2003, A&A, 408, 1137

[49] Zirin H., 1989, Astrophysics of the Sun, Cambridge University Press, Cambridge

Internet Resource

[50] Luttermoser D. G., 2003, Course Notes, http://www.etsu.edu/physics/lutter/courses/astr3415/index.htm

BIOGRAPHICAL INFORMATION

Shilpa obtained her undergraduate degree in Telecommunication Engineering from Bangalore University, India in 2001. Then she joined UTA in fall 2002 for her MS in Electrical Engineering, which she completed in spring 2004. She joined the Department of Physics at UTA the same year in fall, for her MS in Physics. Her field of interest in physics was Astronomy and Astrophysics. She was also the course instructor for two semesters for a freshmen level course, Astronomy I (PHYS 1445), during her enrollment as a graduate student. She completed her MS in Physics in fall 2006.